

1 Evolution of the dynamics, area and ice production of the

2 Amundsen Sea Polynya, Antarctica, 2016-2021

3 Grant J. Macdonald^{1*}, Stephen F. Ackley¹, Alberto M. Mestas-Nuñez¹ and Adrià Blanco-Caba-
4 nillas²

5 ¹⁾ NASA Center for Advanced Measurements in Extreme Environments (CAMEE), University of Texas at
6 San Antonio, San Antonio, TX 78249, USA

7 ²⁾ Department of Geography, University of Victoria, Victoria, BC V8W 2Y2, Canada

8 *Currently at (2)

9 Correspondence to: Grant J. Macdonald (grantmacdonald@uwic.ca)

10

11 **Abstract.** Polynyas are key sites of ice production during the winter and are important sites of biological activity
12 and carbon sequestration during the summer. The Amundsen Sea Polynya (ASP) is the fourth largest Antarctic po-
13 lynya, has recorded the highest primary productivity and lies in an embayment of key oceanographic significance.
14 However, knowledge of its dynamics, and of sub-annual variations in its area and ice production, is limited. In this
15 study we primarily utilize Sentinel-1 SAR imagery, sea ice concentration products and climate reanalysis data, along
16 with bathymetric data, to analyze the ASP over the period November 2016 - March 2021. Specifically, we analyze
17 (i) qualitative changes in the ASP's characteristics and dynamics, and quantitative changes in (ii) summer polynya
18 area, (iii) winter polynya area and ice production. From our analysis of SAR imagery we find that ice produced by
19 the ASP becomes stuck in the vicinity of the polynya and sometimes flows back into the polynya, contributing to its
20 closure and limiting further ice production. The polynya forms westward off a persistent chain of grounded icebergs
21 that are located at the site of a bathymetric high. Grounded icebergs also influence the outflow of ice and facilitate
22 the formation of a 'secondary polynya' at times. Additionally, unlike some polynyas, ice produced by the polynya
23 flows westward after formation, along the coast and into the neighboring sea sector. During the summer and early
24 winter, broader regional sea ice conditions can play an important role in the polynya. The polynya opens in all sum-
25 mers, but record-low sea ice conditions in 2016/17 cause it to become part of the open ocean. During the winter, an
26 average of 78% of ice production occurs in April-May and September-October, but large polynya events often asso-
27 ciated with high, [south-easterly or easterly](#) winds can cause ice production throughout the winter. While passive mi-
28 crowwave data or daily sea ice concentration products remain key for analyzing variations in polynya area and ice
29 production, we find that the ability to directly observe and qualitatively analyze the polynya at a high temporal and
30 spatial resolution with Sentinel-1 imagery provides important insights about the behavior of the polynya that are not
31 possible with those datasets.

32

33

34

35

Formatted: Superscript

Formatted: Font:

Formatted: Font:

Formatted: Indent: First line: 0.25"

Deleted: grant.macdonald@utsa.edu

37 **1. Introduction**

38 Coastal polynyas, or 'latent heat polynyas' (and henceforth referred to simply as 'polynyas'), are sites of
39 open water surrounded by sea ice and land, glacier ice or fast ice (Armstrong, 1972; Tamura et al., 2008; Park et al.,
40 2018). These polynyas are distributed around the coast of Antarctica and are typically at fixed geographic locations
41 each year. They develop because the ice that forms at these sites is regularly driven away by winds or ocean cur-
42 rents, creating an opening in the sea ice (Bromwich and Kurtz, 1984; Bromwich et al., 1993; 1998; Morales
43 Maqueda et al. 2004; Sansiviero et al., 2017).

44 Between the Antarctic summer months of approximately November and March these open water sites tend
45 to remain persistently ice-free. Among other factors, the combination of ice-free conditions, summer sunlight, and
46 the availability of dissolved iron (e.g. Arrigo et al., 2008a; 2012; St-Laurent et al., 2017), enables large phytoplank-
47 ton blooms to develop in polynyas during this summer period. These phytoplankton blooms fix carbon from dis-
48 solved carbon dioxide, some of which then sinks below the surface layer (Sweeney et al., 2003). As a result, the evo-
49 lution of polynyas during the summer is considered a key factor in the primary productivity of the Southern Ocean,
50 and consequently, also their role in the sequestration of carbon dioxide (the 'biological pump') (Arrigo et al.,
51 2008b).

52 Between the Antarctic winter months of approximately April and October polynyas tend to **be** intermit-
53 tently **active** and are smaller in area than in the summer. When a polynya does open during the winter, excess ocean
54 heat is lost and new sea ice production takes place **approximately immediately** in the opened area. Winds (usually
55 katabatic winds) or ocean currents **later** push the newly-produced sea ice away and open the polynya again, **causing**
56 yet more **ice to form**. Repeated polynya 'events' produce new sea ice throughout the winter period and hence polyn-
57 yas have been termed 'factories' of sea ice production (Kimura and Wakatsuchi, 2004; Assmann et al., 2005). Over-
58 all, polynyas are estimated to contribute around 10% of all Antarctic sea ice cover (Tamura et al., 2008; Nihashi and
59 Oshima, 2015). Regionally, polynyas can play an even larger role in production. For example, the Ross Ice Shelf
60 polynya is estimated to produce several cubic kilometers of ice annually, and along with the McMurdo Sound Po-
61 lynya, may produce 20-50% of total sea ice in the region (Drucker et al., 2011). The polynya-produced ice then
62 forms part of the pack ice, contributing to its characteristics and potentially further thickening due to deformation.
63 For example, ice formed by the Terra Nova Bay polynya in the **western** Ross Sea had a mean thickness 3-4 times
64 that of the central Ross Sea, with 80% of the **ice** contained in deformed ice and ridges (Rack et al., 2020). Conse-
65 quently, understanding of polynya evolution through the winter is important for understanding ice production and
66 sea ice characteristics in the Southern Ocean.

67 The Amundsen Sea Polynya (ASP), West Antarctica and the embayment in which it lies are of particular
68 interest for several reasons. The polynya is situated in the embayment into which the Thwaites and Pine Island Glac-
69 iers terminate and undergo ocean-driven melting, making the oceanography of the embayment of special interest
70 (IMBIE team, 2018; Rignot et al., 2019). The ASP is also known to be a key site of primary productivity in the sum-
71 mer, supporting rates of net primary production up to $2.5\text{gC m}^{-2}\text{ day}^{-1}$, the highest for any Antarctic polynya (Arrigo
72 and Van Dijken, 2003; Arrigo et al., 2012), although the level of associated carbon sequestration is unclear (Lee et

Deleted: ¶

Deleted: open

Deleted: then

Deleted:

Deleted: producing

Deleted: sea

Deleted: ice in the open area

Deleted: study area's

84 al., 2017; St-Laurent et al., 2019). Additionally, the ASP has been highlighted as an important site for ice produc-
85 tion. It has been identified as the fourth highest polynya in Antarctica in terms of area and ice production, only be-
86 hind the Ross Ice Shelf, Cape Darnley, and Mertz polynyas (Tamura et al., 2008; 2016; Nihashi and Ohshima, 2015,
87 Nihashi et al., 2017).

88 While there have been several recent studies of the ASP's evolution during the summer months (e.g. Arrigo
89 et al., 2012; Stammerjohn et al., 2015, St-Laurent et al., 2019), knowledge of the ASP and its role in ice production
90 during the winter is limited. Additionally, few studies during the summer have analyzed changes at the sub-monthly
91 scale, and none have observed the polynya directly during cloudy conditions. Aside from one study that analyzed the
92 ASP at the mean monthly scale (Tamura et al., 2016), studies that analyze ice production in the ASP during the win-
93 ter have been limited to estimates of total annual ice production and mean annual area as part of broader-scale cir-
94 cum-Antarctic studies (Tamura et al., 2008; Nihashi and Ohshima, 2015; Nihashi et al., 2017). Other studies of the
95 ASP during the winter have focused on other aspects of the polynya, such as iron and carbon fluxes (St-Laurent et
96 al., 2019). There is a lack of studies of the polynya that characterize changes in the polynya's evolution and area
97 through individual seasons. This is partly due to the difficulty of analyzing polynyas in detail during the polar night.
98 However, the launch of the Sentinel-1 constellation of Synthetic Aperture Radar (SAR) - in full operation by May
99 2016 - enables us to directly observe the polynya during the polar night at a high spatial resolution. Additionally,
100 during the summer light, SAR allows us to make observations regardless of cloud cover.

101 The overall goal of the work presented here is to improve knowledge of the behavior and evolution of the
102 ASP, and thus to aid understanding of recent complex and poorly understood trends in Southern Ocean sea ice con-
103 ditions. This in turn, will aid projections of future changes in Southern Ocean sea condition due to climate change,
104 with important consequences for a range of processes such as Antarctic Ice Sheet stability (Banwell et al., 2017;
105 Webber et al., 2017; Greene et al., 2018; Massom et al., 2018; Arthur et al., 2021) and ecosystem productivity
106 (Grossman and Dieckmann, 1994; Ito et al., 2017). In particular we aim to provide the first qualitative description
107 of the polynya's behavior based on direct observation. The three specific objectives of this paper are to, over the pe-
108 riod November 2016 - March 2021, analyze seasonal and inter-annual (i) qualitative changes in the ASP's character-
109 istics and dynamics, and quantitative changes in (ii) summer polynya area and (iii) winter polynya area and ice pro-
110 duction. The main datasets used are Sentinel-1 SAR images, sea ice concentration products, and climate reanalysis
111 data in the region of the ASP. Additionally, we analyze bathymetric data, and changes in the broader regional sea
112 ice.

113

114 2. Study Site

115 The ASP is located at around $\sim 72\text{-}73^\circ\text{S}$ and $110\text{-}120^\circ\text{W}$ in the Amundsen Sea embayment of the Southern
116 Ocean in West Antarctica (Fig. 1). It is situated in a sector that exhibited an anomalous 40-year decreasing trend in
117 sea ice extent until a 2007 minimum, since which there has been an increasing trend (Parkinson, 2019). The embay-
118 ment also hosts an abundance of icebergs (Mazur et al., 2017; 2019; Bett et al., 2020). To the east, the polynya is
119 bound by the Thwaites Iceberg Tongue (Iceberg B22A; Budge and Long, 2018) and a chain of icebergs grounded
120 over Bear Ridge. To the south, when at its maximum extent, the polynya abuts the Dotson Ice Shelf and part of the

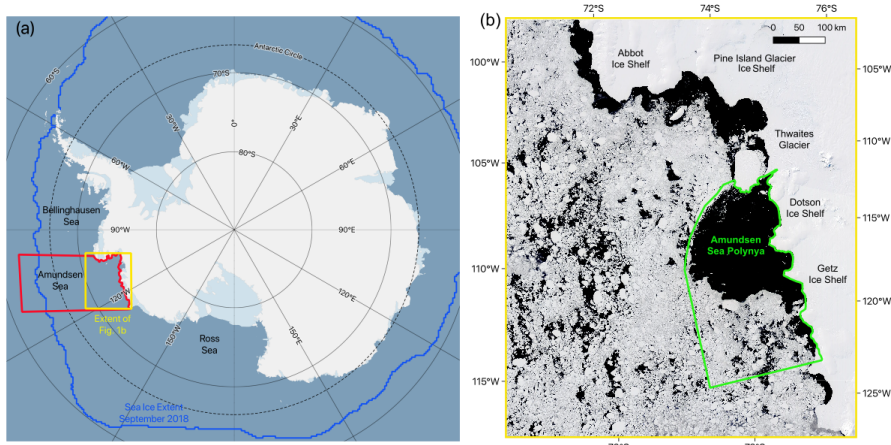
121 Getz Ice Shelf. Immediately east of the eastern boundary of the polynya is an area of ocean that is adjacent to
122 Thwaites Glacier and Pine Island Glacier. The neighboring 'Pine Island Polynya' forms along the coastal stretch
123 around this area and to the north. Westward coastal currents prevail in the area (Kim et al., 2016; St-Laurent et al.,
124 2019), that, along with easterly winds, carry icebergs (Koo et al., 2021) and sea ice into the adjacent sector or the
125 Amundsen Sea and eventually to the Ross Sea (Assmann et al., 2005).

126 The ASP opened every summer during the period 1979-2014 studied by Stammerjohn et al. (2015) and re-
127 tained some open polynya area through the winter period. Arrigo et al. (2012) found no significant secular trend in
128 mean summer open water area between 1997 and 2010, but Stammerjohn et al. (2015) did find the ASP's area in
129 December-February to increase overall over the period 1979-2014. They also noted that the site of the polynya
130 opening shifted to its current typical site adjacent to the Thwaites Glacier Tongue in 1993, having previously been
131 further to the west.

132 Synoptic-scale winds have been found to primarily determine the ASP's area and the timing of opening and
133 closure. Over the period 1997-2010, ASP area was greatest in the summers of 2002-03 and 2009-10, the years with
134 the largest monthly anomalies in easterly and southerly surface winds in the region, and smallest in 2003-04 when
135 there were anomalously high northerly and westerly winds (Arrigo et al., 2012). Polynya summer opening in No-
136 vember was associated with prevailing easterly or southeasterly winds, while closure in March was associated with
137 persistent southeasterly winds at a time when winds promote ice growth in open areas. The polynya was also found
138 to open for summer 16 ± 7 days earlier at the end of the period 1979/80-2013/14 than the beginning (Stammerjohn
139 et al., 2015).

140 During the winter, the **ASP active** area was estimated to have a daily mean of 7700 ± 3600 km² for the pe-
141 riod March-October, 2003-11, as estimated by mapping thin-ice thickness from Advanced Microwave Scanning Ra-
142 diometer for EOS [Earth Observing System] (AMSR-E) data (Nihashi and Ohshima, 2015). Annual ice production
143 volume has been estimated as 92 ± 16 km³ for the period 1992-2001 (Tamura et al., 2008) and 123 ± 24 km³ for the
144 period 1992-2013 (Tamura et al., 2016) by mapping thin-ice thickness using Special Sensor Microwave/Imager
145 (SSM/I) data and calculating heat flux using SSM/I and surface atmospheric data. Nihashi et al., 2017 estimated an-
146 nual volume of ice production, as 90 ± 13 km³ for the period 2003-10, and 90 ± 17 km³ for the period 2013-15, by
147 mapping thin-ice thickness and estimating heat fluxes using AMRS-E and AMSR2 data, respectively.
148

Deleted: polynya's



150
 151 **Fig. 1.** (a) The location of the Amundsen Sea and our study sites within the context of Antarctica and the Southern
 152 Ocean. The background image is from Quantarctica (Matsuoka et al., 2021); (b) The location of the ASP within the
 153 Amundsen Sea embayment. The green boundary indicates the area defined as the ‘ASP study area’ for the purpose
 154 of calculating winter polynya area and ice production. The background image is a true-color MODIS image from 12
 155 December 2020.
 156

157 **3. Data & Methods**

158 **3.1 Qualitative analysis of the ASP’s evolution**

159 In order to qualitatively characterize the seasonal and interannual evolution of the ASP we use Sentinel-1
 160 SAR imagery. Qualitative visual analysis allows us to identify dynamics that are not easy or possible to identify
 161 and/or describe with quantitative data. Sentinel-1 is a constellation of two satellites, A and B, that were launched by
 162 the European Space Agency (ESA) in 2014 and 2016, respectively. The satellite collects radar backscatter imagery
 163 in the C-band which allows observations of sea ice and the ocean during cloudy conditions and the polar night.

164 For our analysis we produced a time-lapse animation in Google Earth Engine using all Sentinel-1 extra-
 165 wide swath (EW) mode, Ground Range Detected (GRD) images over the study site described in section 2 and its
 166 surroundings for the period November 2016 to March 2021. This period was chosen because it includes all the com-
 167 plete summer (November-March) and winter (April-October) periods during which both satellites A and B of the
 168 Sentinel-1 SAR constellation have been active. The EW mode was primarily designed for sea ice and polar zones
 169 and collects images over a wider area than other modes. EW images are available in 20m x 40m spatial resolution
 170 and all images were resampled to 40 m grid spacing. Of four available band combinations (VV, HH, VV+VH, and
 171 HH+HV), we use the HH band because most of the images contain this band. Google Earth Engine applies a series
 172 of pre-processing steps to Sentinel-1 images (<https://developers.google.com/earth-engine/guides/sentinel1>): 1) appli-
 173 cation of orbit file, 2) GRD border noise removal, 3) thermal noise removal, 4) radiometric calibration and 5) or-
 174 thorectification. Images are also converted to decibels (dB). Using these images, we created a time-lapse animation
 175 using Google Earth Engine. This time-lapse included at least partial coverage of the study area for 56 days in 2016,

Deleted: processed

177 359 days in 2017, 341 days in 2018, 317 days in 2019, 329 days in 2020 and 85 days in 2021. In order to analyze
178 particular images in detail, the images were also downloaded from the Alaska Satellite Facility (asf.alaska.edu) and
179 processed in ESA's 'SNAP' toolbox. SNAP was used to crop the images, apply radiometric correction (gamma-
180 nought), apply a Lee (7 x7) speckle filter, and perform ellipsoid correction and map projection, projecting to an Ant-
181 arctic polar stereographic projection. Images were also converted to decibels. The images were then loaded into
182 QGIS (QGIS.org, 2021) for analysis.

183 Qualitative analysis was carried out by visually analyzing the time-lapse videos and images of interest, not-
184 ing changes in the state of the polynya and ice in the region. Visual analysis is possible by analyzing changes in the
185 backscatter signal's texture, pattern and tone and because of the distinct backscatter characteristics of open water,
186 older icepack and different types of thin sea ice. The motion of the ice between images also helped in the identifica-
187 tion of polynya events. Numerous previous studies have noted the ability to observe polynya activity and visually
188 identify polynya opening and the drift of ice with SAR imagery and Sentinel-1 in particular (e.g. Hollands and
189 Dierking, 2016; Dai et al., 2020; Moore et al., 2021). Visual qualitative analysis of SAR imagery also forms an im-
190 portant part of, for example, the Environment Canada's production of sea ice charts (Environment Canada, 2005).
191 Typically, open ocean water has a low backscatter and appears dark, while thicker, older icepack has a relatively
192 high backscatter and appears bright and more granular (we refer to all ice not produced by the ASP as 'pack ice')
193 (Fig. 2a-b). Recently-formed polynya-produced ice has an intermediate backscatter (Fig. 2a). Frazil ice, that may
194 form when a polynya opens up and the open ocean begins to freeze, typically forms in distinct bands of varying
195 brightness (Fig. 2c-d) although it may also form in a 'swirl' or other forms. Open ocean may also appear bright dur-
196 ing high winds, but it is typically clear from the pattern, tone and texture, and the context of the image whether it is
197 an area of ice-free open ocean, or an area of pack ice or active polynya. Incidence angle also influences backscatter
198 and should be considered in a quantitative study of backscatter. Although its effect should be acknowledged, it is not
199 generally considered a significant impediment in the ability to qualitatively analyse dynamics for this study's pur-
200 pose, with visual analysis dependent on a number of factors. Note that what we refer to as 'active' polynya area dur-
201 ing the winter will typically be filled with thin, newly-forming frazil ice.

202 Given the role grounded icebergs play in bounding the ASP, we also downloaded the 'BedMachine Antarc-
203 tica V2' sea floor topography dataset for our study area to examine alongside our qualitative analysis. This dataset
204 was downloaded from the NSIDC (<https://nsidc.org/data/nsidc-0756>) and has a grid spacing of 500 x 500 m
205 (Morlighem et al., 2020).

206 We also use our analysis of the imagery to assess the approximate day of summer polynya 'opening' and
207 'closing'. We deem the polynya to be open for the summer when the open polynya area is primarily free of active
208 ice production, and the day of summer closing to be when the whole open polynya is subject to ice production.

210 3.2 Daily polynya area

211 In order to analyze seasonal and interannual changes in polynya area in summer and winter, daily sea ice
212 concentration (SIC) for the study region was downloaded from the University of Bremen's sea ice data center
213 (seaice.uni-bremen.de). The data was separated into five summer periods from November to March (2016/17,

Deleted:

Deleted: ing

Deleted: and convert the images

Deleted: values

Deleted: signals and texture

Deleted: open

220 2017/18, 2018/19, 2019/20 2020/21) and four winter periods from April to October (2017, 2018, 2019, 2020). This
221 time period was focused on because it coincides with the period for which there is Sentinel-1 A and B data. During
222 the winter we use the term 'active polynya' for areas that we include in the polynya, where an opening has been cre-
223 ated and new ice production is taking place. During the winter we expect thin, frazil ice to immediately begin form-
224 ing when an opening is created (e.g. Nakata et al., 2019; 2021), and thus we prefer the term 'active' to 'open' po-
225 lynya. We begin our winter period in April rather than March because analysis of the Sentinel-1 imagery suggests
226 ice production is not active across the open polynya at the beginning of March. The sea ice concentration product
227 was processed by the University of Bremen using the ARTIST Sea Ice (ASIC) algorithm (Spreen et al, 2008) ap-
228 pplied to AMSR-2 data. AMSR-2 was launched onboard the Japan Aerospace Exploration Agency's (JAXA) Global
229 Change Observation Mission - Water (GCOM-W) satellite in July 2012.

230 We used version 5.4 of the Antarctic-wide, daily sea ice concentration product with no land mask, pro-
231 cessed to 3.125 km grid spacing. This has been used in previous studies to identify polynyas, such as by Moore et
232 al., (2021). This data is of a higher-resolution than data previously used to analyze polynya area in the region. For
233 example, Arrigo et al., (2012) used SSM/I data with 6.25 km grid spacing for their study of summer polynya area.
234 Nihashi et al. (2017) used AMSR-E data with 6.25 km grid spacing for their estimates of ice production. Tamura et
235 al. (2008; 2016) also used SSM/I data, with 12.5 km grid spacing, for estimates of ice production. Stammerjohn et
236 al. (2015) used Bootstrap SIC data with 25 km grid spacing for their analysis of summer polynya area. However,
237 with our higher-resolution data (3.125 km) there remain limitations in using data with such a scale to measure some-
238 thing that can vary on a meterscale. It has been estimated that the ice concentration error in our AMSR-2 dataset is
239 25% at 0% SIC, decreasing to <10% error for SIC over 65% and 5.7% error at 100% SIC (Spreen et al., 2008). It is
240 also noted that the SIC data is known to underestimate SIC where there is thin ice, but as we define an active po-
241 lynya as including thin ice, this is not likely to lead to substantial misclassification of active polynya areas. Data was
242 available for all days in our study period apart from one day in 2019 (1 September).

243 After each day's data was downloaded as a geotiff, it was cropped to the 70 660 km² ASP study area de-
244 fined in Fig. 1b using a shapefile drawn in QGIS with a Sentinel-1 image as reference. Polynya area was then calcu-
245 lated by defining any pixel in the study area with a SIC < 70% as being part of the open polynya. The 70% threshold
246 has been commonly used in other studies of polynyas in the summer (e.g. Parmiggiani, 2006; Morelli & Parmig-
247 giani, 2013; Preußer et al., 2015), and the approach has also been used before to calculate winter polynya area
248 (Cheng et al., 2017; 2019). A limitation is that smaller areas of open water that are represented in a pixel dominated
249 by ice-covered area (i.e. > 70%) will not be included in our polynya area value, while ice-covered areas in pixels
250 with SIC < 70% will be included. However, by comparing our SIC data with the SAR imagery we found applying a
251 70% threshold to the SIC data an effective way of capturing winter, as well as summer polynya area. For example,
252 Fig. 2 b-d shows SAR imagery for a section of the polynya on 21-23 September 2020 and e-g shows the active po-
253 lynya as identified using a 70% threshold with the SIC data for the same days. To further compare the identification
254 of active winter polynya as identified using SIC data with the SAR imagery, we manually identified active polynya
255 in the SAR imagery for the nine days in 2020 when SAR imagery covers the whole ASP study area (green box in
256 Fig. 1b). The results of the comparison can be seen in Fig S1 and generally show good agreement. Note that even if

Deleted: Following other studies (e.g. Dai et al., 2020) d

Deleted: also

Deleted: open

Deleted: However, d

Deleted: note the area is not truly

Deleted: ocean

Deleted: -

Deleted: 'open'

265 ~~the method was perfect there would be a discrepancy because the measurements are taken at different times of day~~
266 ~~and significant changes in active area can occur in hours due to movement of ice, freezing or a mixture of processes.~~
267 ~~There is also an element of human error in the manual measurement. Of the nine cases, the area was identified as~~
268 ~~higher using SIC data in five cases and using SAR data in four cases, suggesting that neither approach leads to a sys-~~
269 ~~tematic over-estimation.~~ Observing Video S2 in comparison to available images in Video S1 also shows the SIC
270 ~~typically effectively captures the presence and variations in area of an active polynya.~~

Deleted: how

Deleted: polynya opening

271 While Sentinel-1 imagery has been used to obtain polynya area during the polar night at a higher spatial
272 resolution (40m, Dai et al., 2020), the Bremen SIC product has three key advantages over using Sentinel-1 SAR im-
273 agery. First, the SIC product is available daily, in contrast to Sentinel-1 which has many, and sometimes prolonged
274 data gaps over the primary area of interest, particularly during June/July. Given that polynya area can change sub-
275 stantially on a daily or hourly timescale, regular gaps of successive days significantly limits the ability to quantita-
276 tively characterize variations throughout the year. Second, several Sentinel-1 images are required to capture the
277 whole ASP study area on a particular day, meaning that even on many days where there are images that are useful
278 for qualitative analysis, the whole polynya cannot be measured. For example, in 2020 there is full coverage ~~of the~~
279 ~~whole ASP study area~~ for only 22 days with none between 26 April and 12 August, ~~and 9 days in winter (although~~
280 ~~there are many other days when the whole polynya itself is visible as it does not extend throughout the whole study~~
281 ~~area).~~ Third, even if sufficient images were available, current methods for calculating polynya area in Sentinel-1 im-
282 agery (e.g. Dai et al., 2020) requires manual delimitation which is labor intensive and would be highly time consum-
283 ing to do for multiple years at a daily temporal resolution. ~~Automated detection of active polynya area in winter us-~~
284 ~~ing SAR is not yet possible to our knowledge.~~

Deleted: .

285 3.3 Daily winter ice production

287 In order to calculate daily ice production in the ASP during the winter periods we followed the approach of
288 Cheng et al. (2017) and utilized their heat flux and ice production model. As input to the model we used atmospheric
289 re-analysis data from the European Centre for Medium-Range Weather Forecasts Reanalysis v5 (ERA5) and the
290 same sea ice concentration data from the University of Bremen described in section 3.2.

291 Hourly ERA5 data, with a spatial resolution of 31 km, was downloaded from Copernicus (cds.climate.co-
292 pernicus.eu; Herbach et al., 2018) for the following meteorological variables: air temperature at a height of 2 m,
293 wind speed at a height of 10 m, surface air pressure, dewpoint temperature at a height of 2 m, downward solar radi-
294 ation and downward thermal radiation. Air temperature, wind speed, surface air pressure and dewpoint temperature
295 were then processed to daily mean values, while solar and thermal radiation were processed to daily cumulative val-
296 ues. These calculations were done for the same ASP study site as for polynya area (Fig. 1b).

298 3.3.1 Heat Flux Calculation

299 Following Cheng et al. (2017) the daily net heat flux, Q (in Wm^{-2}), of an ~~active~~-polynya pixel was esti-
300 mated by:

Deleted: open

β06 $Q = (1 - \alpha)R_i + L_i - L_o + F_s + F_e$ (1)

307

308 where R_i (in Wm^{-2}) is the cumulative downward solar radiation; L_i (in Wm^{-2}) is the cumulative downward thermal
 309 radiation; L_o (in Wm^{-2}) is the upward thermal radiation; F_s (in Wm^{-2}) and F_e (in Wm^{-2}) are the sensible heat flux
 β10 and latent heat flux, respectively; and α is the albedo of open water. α was taken to be 0.06 following Cheng et al.
 311 (2017; 2019), R_i and L_i were taken from the processed daily ERA5 values and L_o , F_s and F_e were calculated as de-
 312 scribed below.

313 The upward thermal radiation was calculated by the Stefan-Boltzmann law:

314

315 $L_o = \varepsilon\sigma T_s^4$ (2)

316

β17 where ε is the longwave emissivity of open water (0.99), and σ is the Stefan-Boltzmann constant (5.67×10^{-8}
 β18 $\text{W}^{-2}\text{K}^{-4}$). The temperature of the water surface (T_s , in K), was assumed to be at the freezing point of seawater (T_0 in
 β19 K), which was calculated following Doherty and Kester (1974) and Cheng et al. (2017; 2019) as:

320

β21 $T_s \sim T_0 = 273.15 - 0.0137 S_w - 0.05199 S_w^2 - 0.00007225 S_w^3$ (3)

322

β23 where S_w (in ‰) is the salinity of sea water. The salinity of the Amundsen Sea was estimated as 34‰ based on Bett
 324 et al. (2020).

325 The sensible heat flux, (F_s), and latent heat flux, (F_e) was calculated by:

326

β27 $F_s = \rho_a c_p C_s U (T_a - T_0)$ (4)

328

329 and

330

β31 $F_e = 0.622 \rho_a L_v C_e U (r e_a - e_s) / P_0$ (5)

332

β33 where ρ_a is the density of air at standard atmospheric pressure and 0°C, taken as, 1.3 kg m^{-3} , c_p is the specific heat of
 334 air at constant pressure, taken as $1004 \text{ J kg}^{-1}\text{K}^{-1}$, U (in ms^{-1}) is the wind speed at 10 m, taken from the processed
 β35 ERA5 data and T_a (in K) is the air temperature at 2 m, taken from the processed ERA5 data. C_s and C_e are bulk
 336 transfer coefficients for sensible heat and latent heat, respectively and both taken as 0.00144. P_0 (in Pa) is the sur-
 337 face air pressure and taken from the processed ERA5 data. L_v (in J kg^{-1}) is the latent heat of water vaporization, r is
 338 the relative humidity. E_a (in Pa) is the saturation water vapor pressure at the air temperature, $r e_a$ is the actual water
 339 vapor pressure of the air and e_s (in Pa) is the saturated water vapor pressure at the surface temperature and are all
 340 calculated below:

341

β42 $L_v = [2.501 - 0.00237(T_s - 273.15)] \times 10^6$ (6)

Deleted: -

Deleted: -

Deleted: A

Formatted: Superscript

Deleted: T_0 (in K), the freezing point of seawater, was assumed to be ...t

Deleted: t

Deleted: -

Deleted: -

Deleted: -

Formatted: Subscript

Formatted: Subscript

Formatted: Subscript

Deleted: -

Formatted: Subscript

Deleted: -

Formatted: Subscript

Deleted: -

Formatted: Subscript

Deleted: -

Deleted: -

358

359
$$e_s = 611.21 \times 10^{0.8094(T_e - 273.15)/(T_e + 0.71)} \quad (7)$$

360

361 and

362

363
$$r_{e_a} = 611.21 \times 10^{0.8094(T_d - 273.15)/(T_d + 0.71)} \quad (8)$$

364

365 where T_d is the dewpoint temperature taken from the processed ERA5 data.

366

367 **3.3.2 Ice production calculation**

368 The calculated daily heat flux was then cropped, re-aligned, resampled to a 3.125 km² grid and reprojected
369 to Antarctic Polar Stereographic using GDAL (Geospatial Data Abstraction Library) and QGIS to match the corre-
370 sponding sea ice concentration data. Next, where SIC was < 0.7 (i.e. pixels considered as part of **active polynya**)
371 daily ice production volume, V , was estimated in km³ following Cheng et al. (2017) by the following equation (9).

372 Although ice production will also take place in non-polynya areas where there is ice cover, here we are only concerned

373 with ice production taking place in the **active polynya**.

374

375
$$V = 3.125^2(1 - SIC)Q/\rho_i L_f \quad (9)$$

376

377 where, as above, SIC is sea ice concentration (as a fraction) and Q is daily net heat flux in W m⁻², ρ_i is sea ice density
378 and taken as 920 kg m⁻³ and L_f is the latent heat of sea ice fusion in J kg⁻¹. L_f is calculated following Moham-
379 med and Nirmal (2015) and Cheng et al. (2017) by:

380

381
$$L_f = 333400 - 2113(T_0 - 273.15) - 114S_i + 18040S_i/(T_0 - 273.15) + 3.35S_i(T_0 - 273.15) - 3.76(T_0 - 273.15)^2 \quad (10)$$

382

383 where S_i is the salinity of sea ice, taken as 6‰ following Cheng et al. (2017).

384

385 Caution should be used when interpreting the absolute numbers produced by the ice production model, particularly
386 because the input data is reanalysis data not necessarily always representative of reality. This is so because
387 the re-analysis itself is a simulation sensitive to uncertain parameter settings, although it is partly corrected by as-
388 simulation of observational data (Cheng et al., 2017; 2019). Also note ERA5 includes a prescribed ‘sea ice area frac-
389 tion’ parameter that influences the interaction between the atmosphere and ocean in the reanalysis. Nevertheless, we
390 opted for this method due to the difficulty of directly measuring and tracking thin ice thickness in the polynya (e.g.
391 Tian et al., 2020) to estimate ice production, and the potential to compare our daily ice production results to results
392 obtained by the same model for the Ross Ice Shelf Polynya (Cheng et al., 2017; 2019).

392

393 **3.4 Broader spatial changes in SIC**

Deleted: .

Deleted: x

Formatted: Font: Italic

Formatted: Superscript

Deleted: open

Deleted: open

398 In order to assess changes in the ASP in the context of changes in SIC at a broader spatial scale, SIC was
 399 analyzed for the larger area defined in Fig. 1a. The same SIC dataset described in section 2.2 to obtain polynya area
 400 was cropped to the broader region. The daily data was plotted spatially for all available days 1 November 2016 – 31
 401 March 2021, as shown in Video S2. Monthly mean SIC was also calculated for the whole period and plotted spa-
 402 tially. Additionally, the total SIC for each day was calculated by calculating the sum of all percentage SIC values in
 403 the study region. These total SIC values should only be considered useful for analyzing relative changes in SIC in
 404 our study period.

406 3.5 Wind analysis

407 In order to analyze the polynya's behavior, we also considered wind conditions. Although a thorough anal-
 408 ysis of wind-vector/ice property correlations is beyond the scope of the present paper, which is primarily focused on
 409 estimating and describing the variability of the polynya's dynamics, area and ice production, we do consider wind
 410 conditions to help inform our analysis of the polynya. Mean daily and annual wind speed and vector winds were cal-
 411 culated from hourly ERA5 reanalysis wind products. Hourly zonal (u) and meridional (v) components of vector
 412 winds at a height of 10 m were obtained from ERA5 for a region adjacent to the Dotson Ice Shelf and iceberg chain
 413 where the polynya typically forms, identified in Fig. S2. Hourly wind speed (V) in ms^{-1} and wind direction (θ) in
 414 degrees were calculated as

$$416 V = (u^2 + v^2)^{1/2} \quad (11)$$

417 and

$$418 \theta = \tan^{-1}(v/u) \quad (12)$$

419
 420 respectively. Daily averaged vector wind fields superimposed on maps of daily averaged wind speed were plotted
 421 for the whole study area for the period 1 November 2016 to 31 December 2020 and are included as supplementary
 422 video Video S3. A wind rose (Fig. 8) showing the wind speed and direction at times when the active polynya both
 423 did not and did increase in area during winter (2017-2020) was also produced for the smaller area (shown by Fig.
 424 S2) where the polynya forms from. A map of annual mean vector wind field superimposed on a map of annual mean
 425 wind speed was plotted in Fig. 9.

426 Unfortunately, there is a lack of local observations of wind data in and around the study area with the clos-
 427 est station in the United States Antarctic Program's database, on Bear Peninsula, lacking wind data for most of our
 428 study period. As a result, some caution should be employed when considering the results obtained from ERA5
 429 winds. However, Bracegirdle (2013) and Stammerjohn et al. (2015) note that data from ERA5's predecessor ERA-I
 430 in the neighboring Bellingshausen Sea performed better than other reanalysis products.

432 4. Results

Deleted: -

Deleted: speed and direction

Deleted: u

Deleted: direction

Deleted: as

Deleted: data

Deleted: u

Deleted: and processed into daily and annual means

Deleted: Fig. S1

Formatted: Font: Italic

Deleted: , V , was

Deleted: ¶

Formatted: Font: Italic

Formatted: Font: Italic, Superscript

Formatted: Font: Not Italic

Deleted: where u and v are ERA5's u and v 10 m wind products, respectively. ...

Deleted: and direction

Deleted: was

Deleted: spatially

Deleted: ,

Deleted: d

Deleted: a

Deleted: , shown by Fig. S2

Deleted: T

Deleted: , t

Deleted: he mean

Deleted: speed

Deleted: and direction

Deleted: s plotted spatially

Deleted: as

Deleted: and as a daily mean speed value

Deleted: for a smaller area where the polynya forms from, shown by Fig. S1...

Deleted: Unfortunately

Deleted: , and

Deleted: s

Deleted: se

467 In this section, we first summarize our qualitative analysis of the polynya dynamics using Sentinel-1 SAR
468 imagery (Video S1) of the ASP between November 2016 and March 2021 (Section 4.1). Second, we analyze quanti-
469 tative changes in summer (November ~~–~~ March) polynya area for the summers of 2016/17 to 2020/21 (Section 4.2).
470 Third, we analyze quantitative changes in winter (April ~~–~~ October) polynya area and ice production for the winters
471 of 2017 to 2020 (Section 4.3). Fourth, we analyze spatial and temporal wind variations and how they relate to po-
472 lynya area (Section 4.4), and finally, we analyze broader regional patterns in sea ice concentration for the period No-
473 vember 2016 ~~–~~ March 2021 (Section 4.5).

Deleted: -

Deleted: -

Deleted: winter

Deleted: in wind speed

Deleted: -

474 475 4.1 Qualitative analysis of ASP using Sentinel-1 SAR imagery

476 Typically, in November or early December the polynya transitions from a winter into summer ‘mode’ as it
477 expands to the west and ice production ceases to take place in the open area i.e. the open polynya area is occupied
478 by open ocean rather than frazil or grease ice (Table 1, Video S1, e.g. Fig 1b). While the polynya’s eastern and
479 southern boundaries remain fixed at the Iceberg Chain and coast, respectively, at times during the summer the po-
480 lynya becomes unbound to the west and/or north, and consequently congruent with the open ocean. In the summers
481 of 2018/19 and 2019/20 it remains bound, but in 2016/17 and 2017/18 substantial openings develop in the pack ice
482 boundary. In the summer of 2016/17, particularly from December, the pack ice in the region is notably sparse in
483 comparison to the other years.

Deleted: Typically

484 In February the pack ice around the polynya becomes more extensive and compact, predominantly due to
485 inflow from the Bellingshausen Sea in the north east. As the new pack ice flows into the area it reforms a west-
486 ern/northern boundary to the polynya in the years where a gap had opened, and in all years pushes the existing pack
487 to the east and south-east, reducing the polynya’s size. In the exceptionally low-pack ice summer of 2016/17, the
488 newly formed boundary of pack ice is remarkably narrow. In March in all years, new ice production can be seen
489 forming in parts of the polynya and is taking place across all of the polynya by the end of March or early April,
490 marking the polynya’s transition into winter ‘mode’ (Table 1).

491 Throughout the winter, polynya ‘events’ occur, with existing ice moving away, predominantly to the west
492 off the Iceberg Chain and Thwaites Iceberg Tongue, and new ice forming in the opening (e.g. Figs. 2b-d). On occa-
493 sion the polynya instead forms to the north off the Dotson Ice Shelf. Between April and August, the main polynya
494 appears to primarily have its maximum extent confined to the area adjacent to the Dotson Ice Shelf. Observation of
495 available imagery of polynya events, along with observation of newly-formed polynya ice outflowing from the area,
496 suggests that there is relatively low ice production in these deep winter months. Early and late in the winter, polynya
497 events are sometimes larger, extending further to the west, and there appears to be more associated ice production.

Deleted: c

Deleted: c

Deleted: August

498 After early winter (March/April), as the area becomes more densely covered by inflowing pack ice and
499 newly-formed polynya ice, obstructions occur that appear to limit the evacuation of polynya-produced ice from the
500 vicinity and limit growth of the polynya. Obstructions particularly take place around and adjacent to a group of per-
501 sistentlly stuck icebergs around the center of the study area that we call the Central Grounded Icebergs around a sea-
502 floor high (Fig. 2a, h). New ice also sometimes becomes stuck (fast) directly adjacent to the south-west of this site
503 (Fig. 2a, h) on another sea-floor high. This intermittently-fast ice blocks outflow from the polynya to the west along

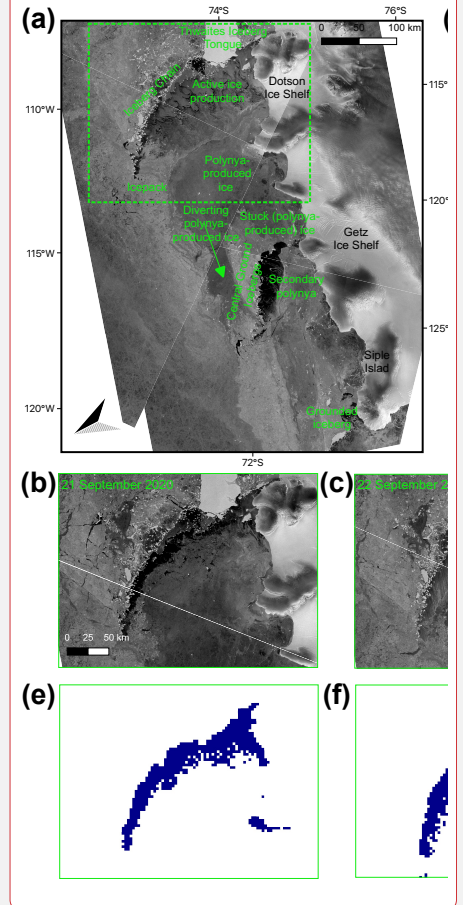
513 the coast, and at times forces new polynya-produced ice to divert around the north of Central Grounded Icebergs
 514 (Fig. 2a). An area of grounded icebergs and intermittently-fast ice by Siple Island also sometimes obstructs ice and
 515 causes diversions further to the north. All ice produced by the polynya flows to the west overall, eventually rounding
 516 the corner of Siple Island.

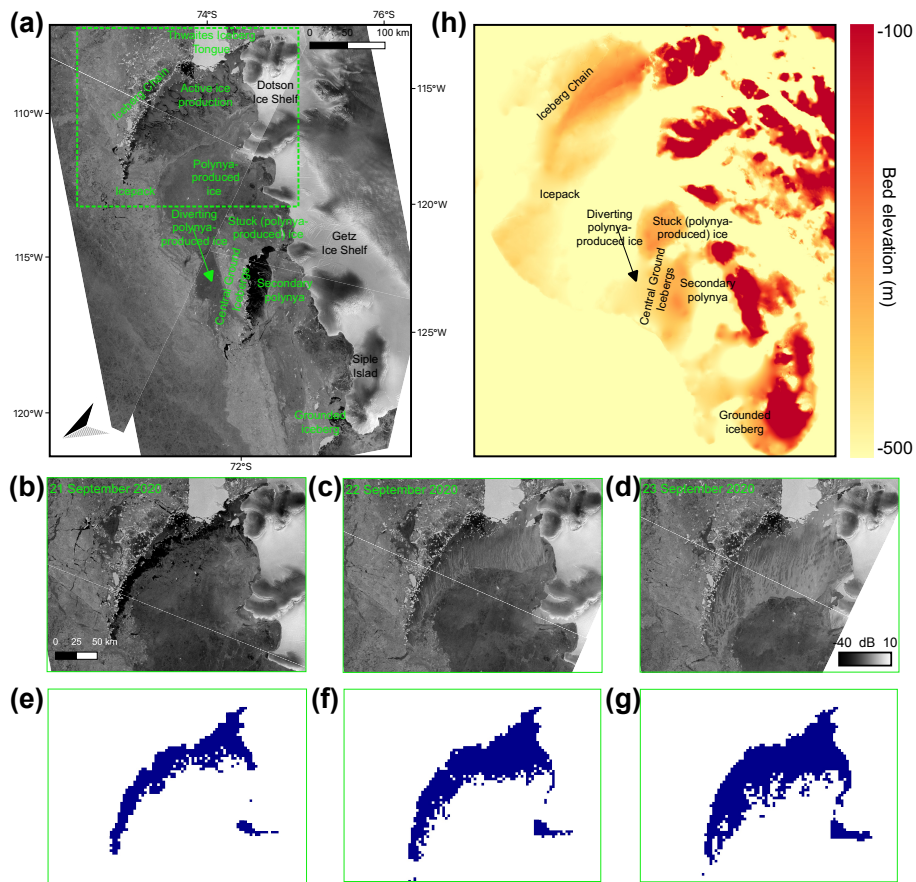
517 We also observe that, while the overall flow of ice from the ASP is to the west, ice flowing from the po-
 518 lynya through the winter ‘heaves’ and regularly temporarily reverses direction, ‘backfilling’ eastward into and to-
 519 wards the polynya (e.g. Fig 3). This means the polynya sometimes closes through backfilling, and not only through
 520 formation and growth of new ice. Back-filling also occur when the polynya does not appear open, meaning that raft-
 521 ing and deformation presumably occurs as ice moves back into the polynya zone.

522 A series of smaller polynyas, other than the main polynya that forms off the Iceberg Chain and Dotson Ice
 523 Shelf, also form within the study area at times. Mostly notably a ‘secondary polynya’ forms at times off the Central
 524 Grounded Icebergs (Fig. 2a). With inflow of ice from the ASP to this area at times obstructed, as ice moves away
 525 from the Central Grounded Icebergs to the west, an opening is created and active ice production is visible. Small
 526 polynyas also form at times to the west off the outcrops along the coast.

527

Deleted: By analyzing Video S1 it is sometimes possible to visually track ice produced by particular polynya events through the season. In particular, in 2020, with some uncertainty due to missing images, we are able to estimate that approximately all of the ice produced between 30 April and 4 November by the main polynya (i.e. excluding the secondary polynya located by the Central Grounded Icebergs) is contained within the red outline in Fig. 4. This section of polynya-produced ice totals 46452 km² in area. →





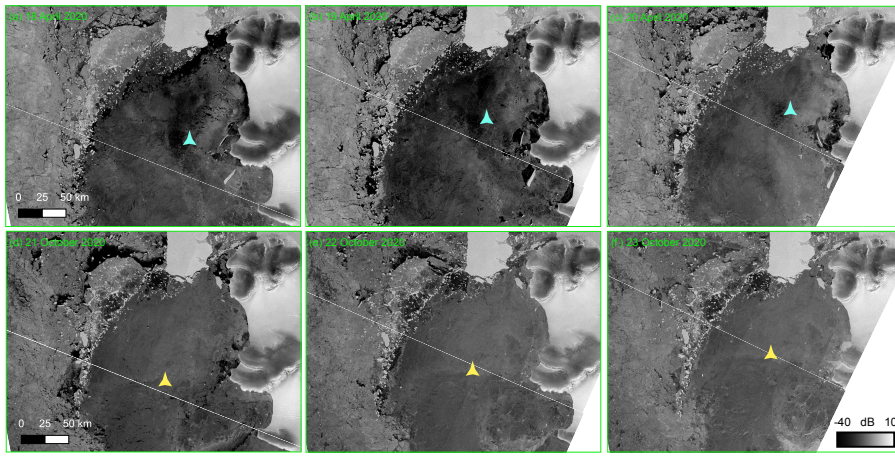
538
 539 **Fig. 2.** (a) An example image of the ASP during the winter in a Sentinel-1 SAR image from 5 September 2019. (b-
 540 d) An example of an active polynya event taking place 21-23 September 2020 in Sentinel-1 SAR imagery. Darker
 541 ice produced by the ASP can be seen diverting around the Central Grounded Icebergs (and some fast pack ice) after
 542 ice became stuck and obstructed outflow along the coast. The area corresponds to the dashed-green box in (a). (e-g)
 543 Active polynya area (blue) for the same dates and areas as b-d as measured by using a 70% threshold with SIC data
 544 (h) The elevation of the bed referenced to mean sea level for the same area as (a). The bathymetry data is from the
 545 MEaSUREs BedMachine version 2 dataset (Mørligheim et al., 2019).

Deleted: Open

546
 547

Year	Polynya opens	Polynya closes
2016/17	8 November 2016*	4 April 2017
2017/18	3 December 2017	9 March 2018
2018/19	13 November 2018	14 March 2019
2019/20	20 November 2019	21 March 2020
2020/21	16 November 2020	8 March 2021

549
550 **Table 1.** Summer polynya opening and closing dates for each summer 2016/17-2020/21 as determined by visual
551 analysis of Sentinel-1 SAR imagery. We determine the polynya to be open for summer when the majority of the
552 open polynya is not exhibiting ice production and closed when the majority of the polynya is exhibiting ice produc-
553 tion. * in 2016/17 a lack of imagery in early November means it is difficult to determine when the polynya opened,
554 but it is open by 8 November.
555

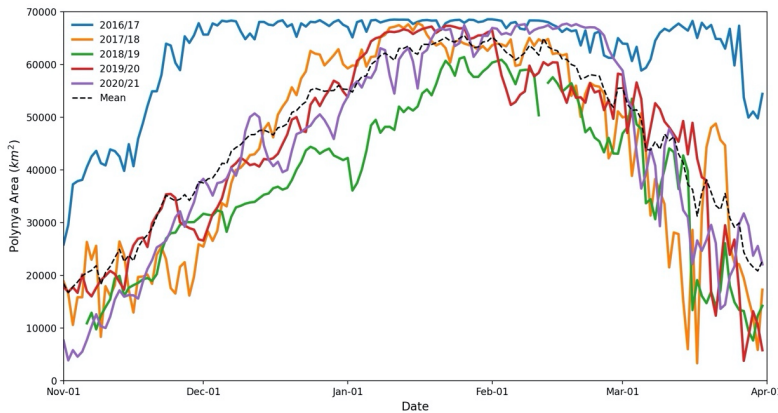


556
557 **Fig. 3** Examples of ‘back-filling’, ice earlier produced by the ASP flowing back towards the area adjacent to the Ice-
558 berg Chain where it formed. Each box corresponds to the same area shown by the dashed-green box in Fig. 2a, (a-c)
559 show the area on 18-20 April 2020, (d-f) show 21-23 October 2020. The colored shapes in each image are in ap-
560 proximately the same relative position within the ice in each set of images and are to help the reader spot the move-
561 ment of the ice through the movement of adjacent features. Other examples of back-filling are visible in Video S1.
562
563

Deleted: <object>

Deleted: <object>

Deleted: ¶
Fig. 4. Ice inside the red boundary is estimated, based on visual analysis of Video S1, to be approximately all the ice produced by the main polynya between 30 April and 4 November 2020. Sentinel-1 SAR image from 4 November 2020.¶



571
 572 **Fig. 4.** Daily summer (November-March) polynya area for each summer 2016/17-2020/21 (solid), and the 5-year
 573 mean of the daily areas for the whole summer period, (dashed).
 574

Deleted: Fig. 5
 Deleted:
 Deleted: mean
 Deleted: for the whole period

575
 576 **4.2 Summer Polynya Area**

577 In all years there is an overall increase in polynya area through November (Fig 4). On 1 November, the po-
 578 lynya has an area between 7 617 km² (2020) and 25 859 km² (2016). In the years 2017/18, 2018/19, 2019/20 and
 579 2020/21 the polynya area follows a similar pattern, but in 2016/17 it follows a distinct course. By 1 December in
 580 2016 the polynya is open in approximately the whole ASP study area, with an area of 65 674 km², an increase of
 581 154% from 1 November. In 2016/17 the polynya remains open across approximately the whole study area through-
 582 out December, January, and most of February and March, only beginning to significantly decline in late March (Fig
 583 4) and into April (Fig 5). The polynya in 2016/17 maintains a higher area than in all other years throughout the
 584 whole summer, apart from a small period in late February when it is surpassed by 2020/21.

Deleted: 1
 Deleted: 813
 Deleted: 19
 Deleted: then

585 In 2017/18, 2018/19, 2019/20, and 2020/21 the polynya area has increased to between 25 439 km² (2017)
 586 and 38 310 km² (2020) by 1 December. From then the polynya continues to follow an overall increasing trend
 587 through December, with the polynya reaching its peak area in January in each of these years. In 2018/19 the peak
 588 area is substantially lower (61 113 km²) than in other years, and the polynya only maintains an area above 60 000
 589 km² for six days in late January and early February. 2018/19 records the lowest area in comparison to other years on
 590 every day between 4 December and 3 February. In 2017/18, 2019/20 and 2020/21 the polynya behaves in a similar
 591 manner through most the period, with no one of those years consistently recording a higher area, and each year
 592 reaching a peak-open area that approximately fills the whole ASP study area. However, polynya area in 2020/21

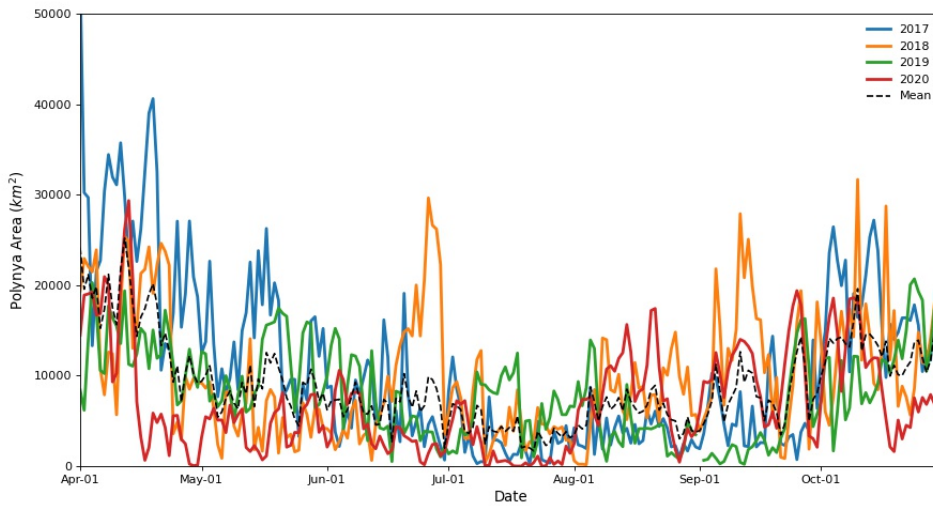
Deleted: 20
 Deleted: 1

603 reaches its peak later (January), and its decline begins later (late February). Notably, in 2017/18 the polynya experi-
 604 ences a temporary rapid re-opening as it increases from just 5 977 km² on 15 March to 48 779 km² on 21 March.
 605 This is an 8.2 fold increase in 6 days, and it is followed by a rapid decline. The polynya had the highest daily mean
 606 area for summer (November-March) in 2016/17, at 62 616 km², and 2018/19 had the lowest, at 38 518 km². The
 607 mean daily area of 2017/18, 2019/20 and 2020/21 for summer was 44 013 km², 44 979 km² and 44 447 km², respec-
 608 tively.

Commented [AM1]: One too many digits here!

Deleted: 7

Deleted: x



609 **Fig. 5.** Daily winter (April-October) polynya area for each winter 2017-2020 (solid), and the 4-year mean of the
 610 daily areas for the whole winter period, as measured from AMSR-2 SIC data (dashed).
 611
 612

Deleted: Fig. 6

Deleted: mean

613 4.3 Winter Polynya Area and Ice Production

614 In all years, polynya area exhibits an overall decline from the beginning of the winter period, when the po-
 615 lynya remains relatively large after the summer period (Fig. 5). This period, when the polynya remains relatively
 616 large but ice production has now begun, accounts for a substantial proportion of the annual ice production (Fig. 6;
 617 Fig. S4). On average, April/May accounts for 36% (39.6 km³) of annual ice production. The polynya then generally
 618 reaches a sustained winter low in area, where it fluctuates around and below 10 000 km². In 2020 the polynya area
 619 reaches its low in early April, while in 2017, 2019 and mean 2017-20 the area continues an overall decline through
 620 April, May and June. Polynya area and ice production then tend to remain low until an increase begins around Sep-
 621 tember. In July polynya area remains below 10 000 km² in all years for the whole month apart from brief small fluc-
 622 tuations above this in 2018 and 2019. There are notable spikes in polynya area in the middle of the year, which are
 623 also exhibited in spikes in ice production. Most notably in June in 2018 polynya area spikes to 26 631 km². After a
 624 period of low polynya area, the area generally increases through September and October towards the summer period.
 625 In 2020 this period of area and ice production increase begins in August. This late-winter increase in polynya area is

Deleted: Fig. 6

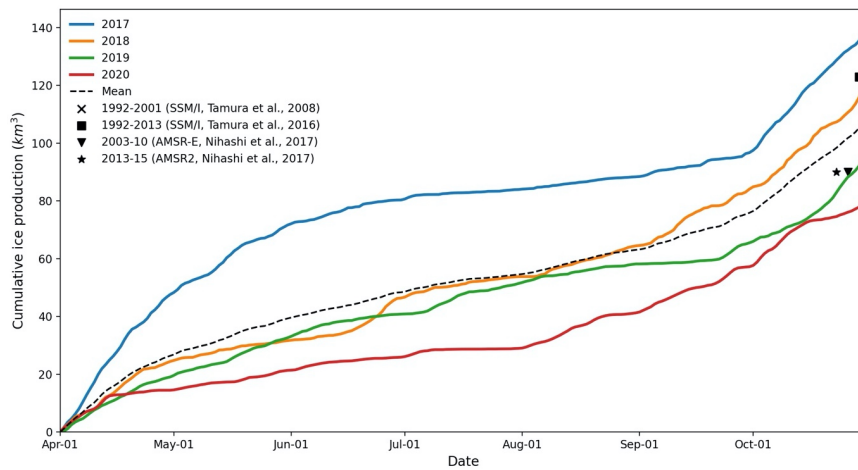
Deleted: Fig. 7

Deleted: Fig. S2

633 also exhibited in a corresponding marked increase in the rate of ice production. On average, September/October ac-
634 counts for 42% (45.8 km³) of annual ice production.

635 We note that in 2017 between the dates of 1 April and 8 May a substantial portion of the calculated **active**,
636 polynya area, and ice production, occurs in the northwest of the ASP study area. This area is part of the open ocean
637 and is separated by sea ice from the more-typically **active** polynya area adjacent to the iceberg chain. Typically, ice-
638 pack fills this northwest area, but in early 2017 it is open due to the lack of icepack in this sector in the summer of
639 2016/17, discussed in section 4.3 (Video S2; Fig. 11b).

640 Analysis of the spatial distribution of ice production across all years reveals that the mean daily ice produc-
641 tion is highest in the area of the polynya adjacent to the Iceberg Chain, Thwaites Iceberg Tongue and Dotson Ice
642 Shelf (Fig. 7). Mean annual ice production values (April-October) in this region surpass 17 m³/m². Other notable
643 areas of higher ice production lie along various parts of the coast and an area that corresponds to the secondary po-
644 lynya by the Central Grounded Icebergs.



645 **Fig. 6.** Daily cumulative winter ice production for each winter (April-October) 2017-2020 (solid), and the 4-year
646 mean for the period (dashed), as measured using heat-flux modeling of ERA-5 data and AMSR-2 SIC data. Also
647 shown are mean annual measurements for 1992-2001 (Tamura et al., 2008), 1992-2013 (Tamura et al., 2016), 2003-
648 10 and 2013-15 (Nihashi et al., 2017), along with the instrument used for each measurement. Note the previous stud-
649 ies' measurements covered the period March-October and used a study area that does not exactly correspond to ours.
650
651
652

Deleted: open

Deleted: open

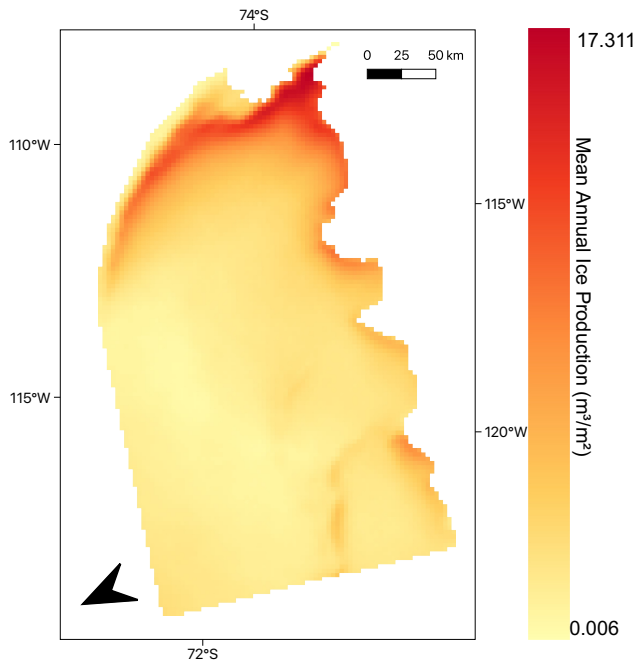
Deleted: Fig. 8

Deleted: Fig. 7

Deleted:

Year	Mean Daily Active Polynya Area (km ²)	Total Annual Ice Production (km ³)	Total Mean Daily Ice Production (km ³)
2017	10 908 (9589)	139	0.67 (0.67)
2018	9 963 (7004)	121	0.57 (0.50)
2019	8 152 (5127)	95	0.45 (0.38)
2020	6 910 (5692)	80	0.38 (0.36)
Mean 2017-20	8 984 (7240)	109	0.52 (0.51)

Table 2. Estimates of Mean Daily **Active** Polynya Area, Total Annual Ice Production and Mean Daily Ice Production during the winters of 2017-2020, and for the daily mean of the period. Numbers in brackets indicate the standard deviation.



658 **Fig. 7.** Mean Annual Ice Production for all winter study periods (April-October 2017-2020). The region corresponds
659 to the region within the green outline in Fig. 1b

Deleted: Fig. 8

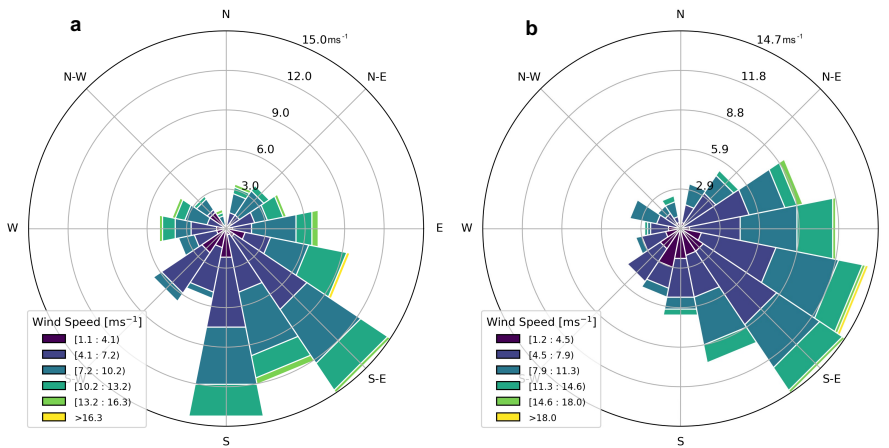
660 **4.4 Wind and polynya area**

661 It is clear that polynya events are associated with the presence of strong south-easterly and easterly winds
662 in the region. Figs. 8-9 show that south-easterly and easterly winds dominate the polynya study area. Comparing
663 winter winds in the region where the polynya forms from (Fig. 8; S2) when the active polynya does not increase in
664 area and when it does, shows that while south-easterly winds often occur in both instances, there is a stronger east-
665 erly component when an increase in area occurs. The top three wind directions associated with a daily increase in
666 active polynya area are south-easterly, east-south-easterly and easterly, whereas they are south-easterly, southerly
667 and south-south-easterly when area does not increase. Fig. S3 also shows the high density of active polynya area
668 increases with winds with a southerly/easterly winds. It is also clear from Fig. 9 that the location of polynya for-
669 mation is associated with a band of high winds with a mean speed of around 8 – 9 ms⁻¹ exists along the coast from
670 Thwaites Glacier, over the Thwaites Iceberg Tongue and into the eastern area of the ASP study area. In the western
671 part of the study area that the polynya extends into, winds tend to be more easterly than south-easterly. Although
672 many day-to-day variations in polynya area are not necessarily associated with high wind speed, it is clear that nota-
673 ble spikes in polynya area do often occur on days with high wind speed (Fig. S5).

Deleted: s

Deleted: not

674

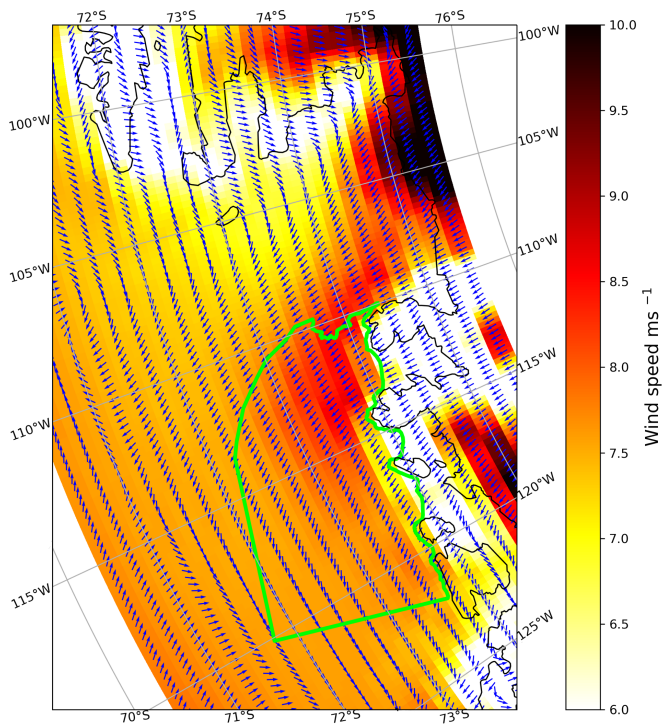


Deleted: Although it appears many day-to-day variations in polynya area are not correlated with wind speed, it is clear that notable spikes in polynya area do often occur on days with high wind speed (Fig. S3), particularly when there is an easterly component (Video S3). For example, the three highest polynya areas recorded in 2020 after April all occur alongside the three highest spikes in wind speed post-April. By viewing the mean spatial distribution of winds, it is clear that the ASP forms in an area of relatively high winds that often have an easterly component (Fig. 9). A band of high winds with a mean speed of around 8 - 9 ms⁻¹ exists along the coast from Thwaites Glacier, over the Thwaites Iceberg Tongue and into the eastern area of the ASP study area, where the main polynya originates. ¶

675

676 **Fig. 8.** Wind roses showing the distribution of wind speed and direction during all winters (April-October) in the
677 study period, when the active polynya (a) did not increase in area and (b) did increase in area. These winds are cal-
678 culated for a region close around that the iceberg chain that the polynya forms from, shown by Fig. S2.

Formatted: Font: Bold

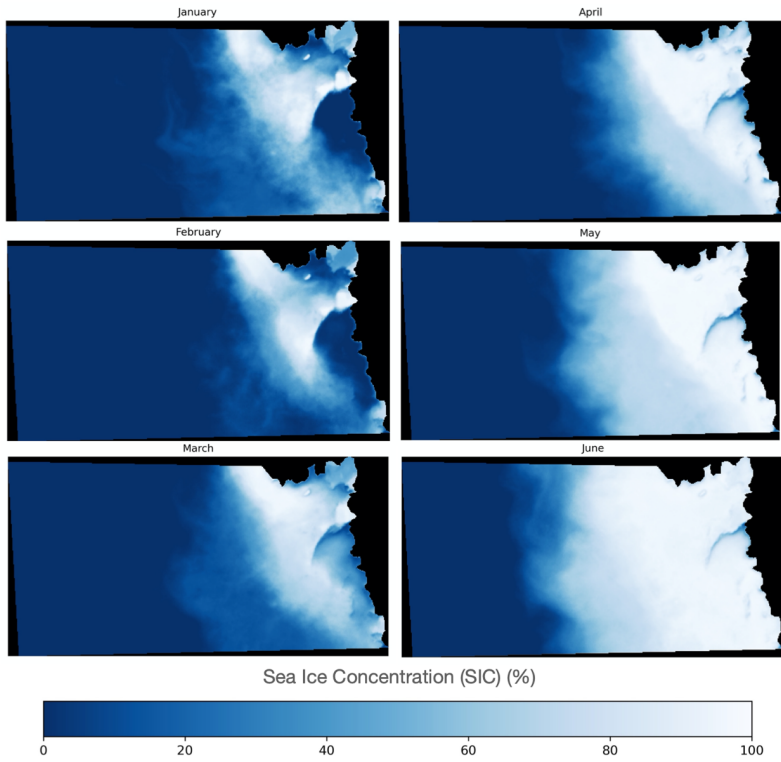


695
696
697
698
699
700
701
702
703

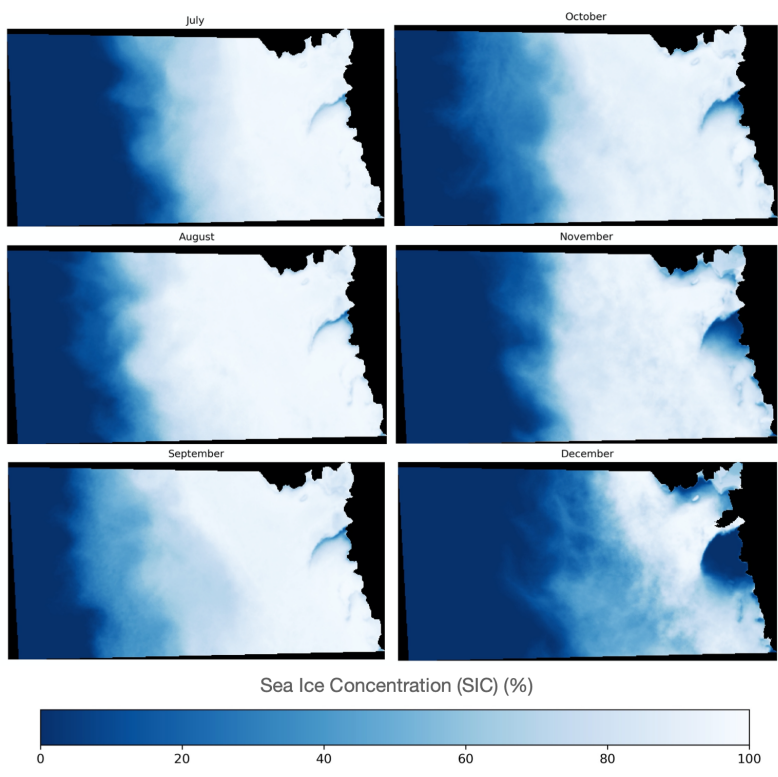
Fig. 9. Annual mean vector wind field and wind speed, calculated for the period 1 November 2016 to 31 December 2020. The green boundary represents the ASP study area, also shown in Fig 1b. Daily maps of vector wind fields and wind speed are included as Video S3.

- Deleted: Mean a
- Deleted: speed and direction
- Deleted: ox
- Deleted: the
- Deleted: same
- Deleted: as the green box
- Deleted: Daily
- Deleted: and direction
- Deleted: is

713



714
715
716
717
718
719
720
721
722
723
724
725
726
727

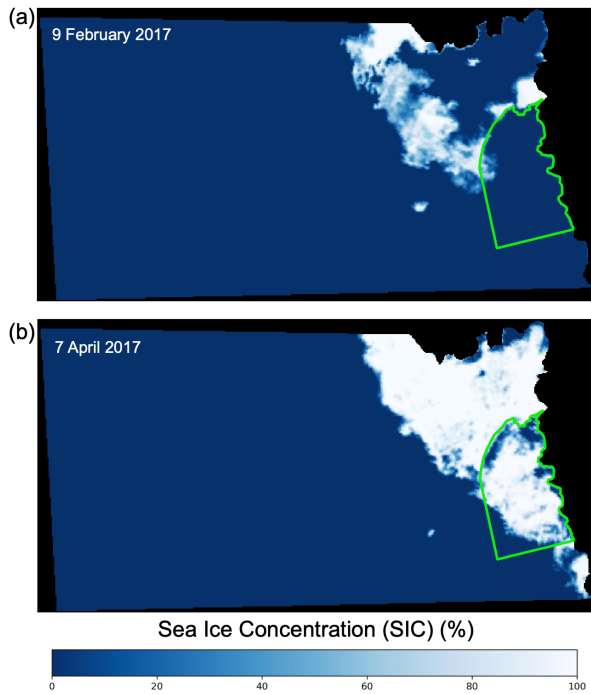


728 **Fig. 10.** Mean monthly SIC for the broader ASP region for the period November 2016 to March 2021. The area cor-
 729 responds to that shown by red box in Fig. 1a. Daily data is shown in Video S2.

Deleted: <object>

730
 731
 732
 733
 734
 735
 736
 737
 738
 739
 740

742



743

744 **Fig. 11.** SIC for the broader ASP region on two days in 2017, during and following a summer of record-low SIC. (a)
745 An example of when the polynya had no sea ice boundary to the west/north-west due to the exceptionally low SIC in
746 the region during the 2016/17 summer. (b) An example of the low SIC in the region early in the subsequent winter,
747 when only a narrow area of pack ice and polynya ice fills the area. The area corresponds to that shown by red box in
748 Fig. 1a.

749

750 4.5 Broader SIC

751 Analysis of the SIC over a broader area also shows daily changes in the polynya area and how it relates to
752 changes in the icepack. The mean monthly cycle of the polynya can be seen in Fig. 10 and presents a similar picture
753 of the polynya as described in sections 4.1- 4.3. The broader icepack has a minimum total SIC in January and re-
754 mains similar in February. From March the broader icepack can be seen to expand in area as the polynya begins to
755 close and continues to increase until a peak SIC in September. From October the icepack begins a marked decline

756 into summer. Interannual variation can be seen in [Fig. S6](#) and Video S2, with maximum icepack area occurring in
757 August or September each year, and minimum icepack in January or February.

758 During the summer of 2016/17 the icepack is notably sparse (Fig. 11; [S6](#)). Around 29 December 2016 a
759 gap in the icepack connects the ASP to the open ocean to north. The icepack continues to diminish and the gap con-
760 necting the ASP to the open ocean broadens until by February the polynya is only bound by part of the Iceberg
761 Chain and Thwaites Iceberg Tongue. The total SIC reaches a minimum on 5 February 2017, 35% of the next lowest
762 annual minimum (2019/20). Gaps in icepack around the Iceberg Chain mean that the ASP has essentially joined
763 with the Pine Island Polynya through the Iceberg Chain for a period in this year. The narrow band of icepack from
764 the east closes the polynya off again in March but the band of adjacent icepack remains so narrow that, as men-
765 tioned, there is open ocean inside our ASP study area until 9 May (Video S2).

767 5. Discussion

768 Our analysis shows that in some ways the ASP, between November 2016 and March 2021, behaves as is
769 typical for Antarctic coastal polynyas. During the summer the polynya becomes larger and remains ice-free ([Fig. 4](#),
770 Video S1), while during the winter it becomes smaller, opening up during ice-producing polynya ‘events’ (Figs. ~~4~~[5](#),
771 Video S1). These polynya events and changes in polynya area can sometimes be attributed to higher wind speeds
772 [and are often associated with a stronger easterly component in winds close to the iceberg chain](#) (Figs ~~7~~[9](#), S3).

773 Our qualitative analysis of Sentinel-1 SAR imagery, however, also reveals distinct characteristics of the
774 ASP which are not possible to decipher from sea ice concentration data, other quantitative methods, or indirect ob-
775 servation. First, we note that while in many other polynyas, such as the Ross Ice Shelf Polynya, new polynya-pro-
776 duced ice is typically efficiently evacuated away from its origin (Dai et al., 2020), this is not the case at the ASP.
777 Instead, ice formed by the ASP often remains in the ASP study area for months (Video S1). In fact, this polynya-
778 produced ice does not consistently flow in a direction away from the polynya. While its overall direction is west-
779 ward, away from the polynya, the ice ‘heaves’ and temporarily flows ‘backward’ (‘back-fills’) (Fig. 3), as has also
780 been observed at the Mertz Glacier Polynya (Massom et al., 2017). The ice also gets ‘stuck’ in the region, particu-
781 larly around grounded icebergs, which are grounded in areas where there are topographic highs in the sea floor (Fig.
782 2a, h).

783 The tendency of ice produced by the ASP to remain in the vicinity of the polynya for prolonged periods,
784 become stuck, and sometimes flow back eastward towards the site of its formation, influences the polynya and ice
785 production in two key ways. First, when ice moves eastward while the polynya is [active](#), it contributes to the closure
786 of the polynya, and thus the cessation of ice production. Typically, it is assumed that an [active](#) polynya during win-
787 ter closes due to new ice production (e.g. Cheng et al., 2017). However, the ASP may close both due to ice produc-
788 tion and movement of previously-produced ice into the polynya. Second, we suggest that the blockages of ice in the
789 vicinity of the polynya reduce the size and frequency of polynya events by hindering the ability of ice to move out of
790 the polynya and open it up. Again, by reducing the size and duration of [active](#) polynya area during winter, ice pro-
791 duction is limited.

Deleted: Fig. S4

Deleted: 4

Deleted: Fig. 5

Deleted: 5

Deleted: 6

Deleted: 8

Deleted: , Fig. 4

Deleted: open

Deleted: open

Deleted: open

802 We also note that the ASP forms along the coast westward off a chain of icebergs that extend from the
803 Thwaites Iceberg Tongue. While some polynyas, such as the Ross Ice Shelf polynya, form off and away from the
804 coast, the majority of Antarctic polynyas have been shown to form westward off glacier ice tongues or protruding
805 fast ice (Nihashi et al., 2017). In the case of the ASP, its location and orientation is determined by the presence of
806 the 'Iceberg Chain', which is in turn determined by the presence of a bathymetric high (Figs. 1-2). Stammerjohn et
807 al. (2015) refer to the polynya as forming off a 'fast ice tongue' but we prefer to refer to the 'Iceberg Chain' as the
808 eastern boundary. While a section of fast ice exists amongst, and adjacent to, a section of the southern part of the
809 Iceberg Chain, the extent of this fast ice varies and it only ever extends along a portion of the Iceberg Chain. The
810 Iceberg Chain remains virtually the same length throughout our observations. The polynya consistently forms off the
811 Iceberg Chain regardless of the state or extent of the fast ice. This means that, unlike polynyas that form off variable
812 fast ice (Nihashi et al., 2017), the fundamental morphology of the ASP remains stable through the period. We also
813 note that at no point do we observe significant portions of icepack to 'break through' the Iceberg Chain from the
814 east, regardless of the state of fast ice extent or conditions, and thus the icebergs and the bathymetric high persistently
815 'shield' the polynya from icepack inflow.

816 Another notable feature of the ASP is the development of a 'secondary polynya' during the winter (Fig.
817 2a), where ice production also takes place. This is a polynya that forms within the ASP study area, in an area that is
818 usually part of the main ASP during the summer, but it is not typically congruent with the 'main' polynya during the
819 winter. The polynya forms at the site of the 'Central Grounded Icebergs' and associated 'stuck', transient fast ice.
820 Because some ice has become stuck over the bathymetric high, when adjacent ice drifts away, a polynya **activates**.
821 This feature again highlights the significance of the bathymetry of the region for sea ice production and dynamics.

822 In line with previous studies of the ASP we find that the ASP is an important site of ice production
823 throughout the winter. Our estimates of annual ice production for 2019 and the mean for 2017-20 fall within the
824 range of predictions by Tamura et al. (2008; 2016) and Ohshima et al. (2017) for 1992-2001/2003-10/2013-15 (90 -
825 117km³) (Fig. 6). Our estimates for total annual ice production for 2017 (139 km³) and 2018 (121 km³) are higher
826 than the highest estimate of those studies, while for 2020 (80 km³) it is lower. This suggests no significant trend in
827 interannual ice production can be discerned from comparing the period of our study to these previous studies. Some
828 caution must be used in this comparison, however, because those studies include March in ice production calcula-
829 tions and our ASP study area does not exactly correspond to theirs.

830 We find that the shoulder seasons of April/May and September/October are particularly important for ice
831 production due to the higher polynya area at these times, accounting for 36% and 42% of the annual ice production,
832 respectively. This is particularly the case in 2017, when an exceptionally high open polynya area in the summer, due
833 to low icepack conditions (discussed below), continues into the winter period (Figs. 4-6). However, we show that at
834 least some polynya area **activates** and some ice production occurs throughout the whole winter (Figs. 5-9). Addition-
835 ally, there can be spikes in polynya area and ice production in the deepest winter months. Most notably, polynya
836 area reaches 26 631 km² in June. Such isolated, winter events are not reflected in the daily mean for the whole study
837 period, but only when analyzing daily changes for each year (Fig. 5), highlighting the importance of analyzing po-
838 lynya area and ice production at the daily scale to discern important polynya dynamics.

Deleted: opens

Deleted: Fig. 7

Deleted: 5

Deleted: 7

Deleted: opens

Deleted: 6

Deleted: 7

Deleted: Fig. 6

847 When comparing our results to those of Cheng et al. (2017), who used the same method for calculating ice
848 production at the Ross Ice Shelf Polynya, we find that the ASP produces substantially less ice. Between 2003 and
849 2015 they found ice production for the Ross Ice Shelf Polynya was between 164 and 313 km³ (also for April - Octo-
850 ber) compared to 80 to 139 km³ for the Amundsen Sea Polynya (this study). This is in line with other studies that
851 compare the two polynyas (Tamura et al. 2008; 2016; Nihashi et al. 2017). We suggest that one limit on polynya
852 area and ice production for the ASP compared to the larger Ross Ice Shelf Polynya, is that the ASP typically forms
853 off the Iceberg Chain. The Iceberg Chain has a stable length of ~190 km, limited by the length of the seafloor sill on
854 which it is grounded, and is an upper limit on the polynya in one dimension. The Ross Ice Shelf Polynya, on the
855 other hand, forms off a coastline, and is only typically limited in this spatial dimension by weather/oceanographic
856 conditions. Another comparative limit on the ASP's ice production is the previously discussed tendency for po-
857 lynya-produced ice to inhibit further activation of the polynya due to blockages and reversals in ice drift. This pro-
858 cess could also partly explain why Cheng et al. (2017) found ice production to remain relatively consistent through-
859 out the winter for the Ross Ice Shelf Polynya, whereas we find ice production for the ASP in June-August to be
860 much lower than in the shoulder months of April/May and September/October.

861 We also note the polynya-produced ice leaves our study area and enters the adjacent sector of the Amund-
862 sen Sea to the west, rather than traveling away from the coast after formation. This westward flow of the ice away
863 from the polynya is likely, in this section, primarily due to the prevalence of easterly winds, especially towards the
864 western part of the study area, and westward ocean currents in the region (Kim et al., 2016; St-Laurent et al., 2019).
865 These ocean currents have been shown to carry icebergs away from our study region, westward through the Amund-
866 sen Sea and into the Ross Sea (Koo et al., 2021). Broader prevailing easterly winds likely play a dominant role in
867 sea ice produced by the ASP eventually drifting to the Ross Sea, as part of a coastal band of westward ice drift (Ass-
868 mann et al., 2005). The fact that the polynya-produced ice remains by the coast may also be influenced by the inflow
869 of older, thicker icepack into our study area. Icepack appears to flow into the region from the Bellingshausen Sea
870 (Video S1, S2) and flows parallel to the ASP-produced ice, potentially playing some role in 'trapping' the ice by the
871 coast. The westward flow of the ice suggests that the level of ice production in the ASP is significant for the adja-
872 cent sector of the Amundsen Sea and the Ross Sea.

873 During the summer we observe the ASP to behave in a similar way in 2016/17 - 2020/21 as Stammerjohn
874 et al. (2015) showed for the period 1979 - 2014. As they did, we find the polynya to open every summer during our
875 study period. We do not note any shift in the location of opening, with the location remaining in the same place as
876 Stammerjohn et al. (2015) noted that it had shifted to in 1992/93. As they did for the years 1992, 1993, 1995, 1997,
877 2003, and 2010, we also note that in 2016/17, there is no icepack adjacent to the ASP in the north and west. This is
878 due to limited advection from the Bellingshausen Sea and Pine Island Polynya, and it causes the ASP to become
879 congruent with the open ocean (Fig. 11). This year was noted as a year of unprecedented springtime retreat and low
880 sea ice concentration for Antarctic sea ice, and was associated with a series of record atmospheric circulation anom-
881 alies and sea surface temperatures (Turner et al., 2017). These broader sea ice conditions caused the polynya to be
882 open in approximately the whole ASP study area through most of the summer in 2016/17, from late November to

Deleted: opening

884 March. During this time there is also little-to-no distinction between the ASP and the neighboring Pine Island Po-
885 lynya, other than the presence of the Iceberg Chain (Fig. 11a, Video S1). The effect of these extraordinary sea ice
886 conditions in 2016/17 on the polynya in summer, and early winter as mentioned above, may offer insight into how
887 the ASP will behave more commonly in the future if climate change makes such conditions more likely.

888 We note that while Stammerjohn et al. (2015) found the largest polynya area to be February in all but two
889 years during 1979 - 2014, we find the polynya area to be highest in January in each year apart from 2016/17 (when it
890 reaches the peak in November) (Fig. 4). Arrigo et al. (2012) also generally found the polynya area to increase until a
891 later peak in February for the years 1997/98 - 2009/10. While there should be some caution in directly comparing
892 our results with those, due to varying datasets, methods and definitions of the study area, we suggest that a shift in
893 the timing of maximum summer area would promote primary productivity in the polynya. Arrigo et al. (2012) found
894 primary productivity (per unit area) to typically peak in January, and to be declining by the time of the polynya area
895 peak. If the polynya reaches a higher area at an earlier time, when primary productivity is higher, we suggest the
896 potential for primary productivity may be larger during our study period.

897

898 6. Conclusions

899 Focusing on the summers of 2016/17 - 2020/21 and the winters of 2017 - 2020, we present the first detailed
900 study of year-round variations in the Amundsen Sea Polynya's behavior, area, and ice production. In particular, we
901 take advantage of the recent availability of Sentinel-1 SAR imagery to qualitatively assess the dynamics of the po-
902 lynya through the whole year.

903 Our findings agree with previous studies of earlier periods in finding that the ASP produces a substantial
904 amount of ice through the winter, with some inter-annual variation. We add that the shoulder seasons of April/May
905 and September/October dominate winter ice production, contributing a combined 78%. However, large polynya
906 events, often associated with high winds and a stronger easterly component in wind direction, can occur throughout
907 the winter, promoting significant ice production.

908 The ASP opens each summer in November and closes in March or early April, with peak area typically oc-
909 ccurring in January. We find that broader regional sea ice conditions can play an important role in the polynya in
910 summer, with the record-low sea ice extent in 2016/17 causing the ASP to become part of the open ocean to the
911 north and join with the Pine Island Polynya to the east.

912 Through our qualitative assessment we identify that the ASP behaves in a distinct manner. The polynya
913 typically forms in a westward direction off a persistent chain of grounded icebergs that are grounded along a bathy-
914 metric high. Ice produced by the polynya is not efficiently evacuated from the site as with other polynyas such as the
915 Ross Ice Shelf Polynya. Instead it stays within the study site, typically for months through the winter, sometimes
916 becoming stuck. This behavior is related to local topographic sea-floor highs which cause icebergs to become
917 grounded and ice to become stuck. At times another smaller 'secondary polynya' forms within the study area adja-
918 cent to grounded icebergs. Relatedly, ice produced by the polynya does not consistently move away from the ASP,
919 instead 'heaving' and sometimes drifting back towards it, contributing to its closure and limiting ice production. Un-
920 like some other polynyas, the polynya-produced ice also drifts westward into other sectors, instead of north, away

Deleted: Fig. 5

922 from the coast. These behaviors should be accounted for when considering the ASP's influence on the region's sea
923 ice, biology and oceanography.

924 Given temporal and spatial gaps in Sentinel-1 SAR's coverage, and the difficulty in automating polynya-
925 identification in SAR data, we do not find that it can replace passive microwave or sea ice concentration datasets for
926 analyzing daily changes in polynya area or ice production. However, we find that the ability to directly observe and
927 qualitatively analyze the polynya at a high spatial and temporal resolution, year-round, with Sentinel-1 imagery pro-
928 vides important insights that are not possible with those other datasets. Development of automated approaches to
929 also use Sentinel-1 to quantify high-spatial resolution changes in polynya area and state, such as through machine-
930 learning, could extract more potential from the datasets, particularly for regions with fewer temporal and spatial
931 gaps. Combining such an approach with ice-tracking algorithms to track ice produced by polynya events and meas-
932 urements of ice thickness (e.g. from satellite altimetry), could help further quantify ice production by polynyas.

934 *Code and Data Availability*

935 Code for data processing and production of figures and videos is available at
936 <https://github.com/georgeordie/AmundsenSeaPolynyaPaper>. All processing was done with freely available software,
937 and all data is freely available. Sentinel-1 images were processed in Google Earth Engine or downloaded from:
938 asf.alaska.edu. BedMachine Antarctica V2 was downloaded from: <https://nsidc.org/data/nsidc-0756>. Sea ice concen-
939 tration data was downloaded from: <http://seaice.uni-bremen.de/>. ERA5 climate data was downloaded from:
940 <https://cds.climate.copernicus.eu>. The MODIS image used for Fig. 1b was downloaded from:
941 <https://worldview.earthdata.nasa.gov/>

943 *Video Supplement*

944 Video S1: <https://doi.org/10.5281/zenodo.5179444>

945 Video S2: <https://doi.org/10.5281/zenodo.5179509>

946 Video S3: <https://doi.org/10.5281/zenodo.5179590>

948 *Author Contributions*

949 GJM primarily conceived the study, processed and analyzed all data and produced all figures, apart from some of
950 the wind processing, analysis, and figures done by AB-C. SFA and AMM-N also contributed to the design of the
951 study and all authors discussed the results and were involved in editing the manuscript.

953 *Competing Interests*

954 The authors declare that they have no conflict of interest.

956 *Financial Support*

957 This work was supported by NASA grant #80NSSC19M0194.

Deleted: We also note that it is sometimes possible to visu-
ally-track ice created by particular polynya events for several
months as it drift...s.
s.

Deleted: s.

Deleted: Employing i

Deleted: in Sentinel-1 images, with

Deleted: and extract more potential from Sentinel-1 da-
tasets...

967
968
969
970
971
972
973
974
975
976
977
978
979
980
981
982
983
984
985
986
987
988
989
990
991
992
993
994
995
996
997
998
999
1000
1001
1002
1003
1004
1005
1006
1007
1008
1009
1010
1011
1012
1013
1014
1015

Acknowledgements

We gratefully acknowledge the European Space Agency for making available Sentinel-1 data and the SNAP toolbox, and Google Earth Engine for hosting and processing Sentinel-1 data. We acknowledge the free package Quantarctica, developed by the Norwegian Polar Institute, for use in Fig. 1a. We thank the University of Bremen Sea Ice Remote Sensing Group for processing and making available their sea ice concentration product and the Japanese Space Exploration Agency for launching and managing AMSR2. We also acknowledge the ECMWF, NSIDC and NASA for freely-available data. Among others, the free, open-source software packages QGIS, GDAL, Python, NumPy and Matplotlib were invaluable in this research. We also thank the GIS and StackOverflow StackExchange communities for resources that aided data processing. We thank three anonymous reviewers who reviewed an earlier draft of this paper and editor Nicolas Jourdain for suggested minor revisions.

References

Armstrong, T.: World meteorological organization: WMO sea-ice nomenclature. Terminology, codes and illustrated glossary. *J. Glaciol.*, 11, 148–149. <https://doi.org/10.3189/S0022143000022577>, 1972.

Arrigo, K. R., van Dijken, G. L., and Bushinsky, S.: Primary production in the Southern Ocean, 1997–2006. *J. Geophys. Res.*, 113, C08004. <https://doi.org/10.1029/2007JC004551>, 2008a.

Arrigo, K. R., van Dijken, G. L., and Long, M.: Coastal Southern Ocean: A strong anthropogenic CO₂ sink. *Geophys. Res. Lett.*, 35, L21602. <https://doi.org/10.1029/2008GL035624>, 2008b.

Arrigo, K. R., Lowry, K. E., and van Dijken, G. L.: Annual changes in sea ice and phytoplankton in polynyas of the Amundsen Sea, Antarctica. *Deep Sea Research, II* 71–76: 5–15. <https://doi.org/10.1016/j.dsr2.2012.03.006>, 2012.

Arrigo, K. R. and van Dijken, G. L.: Phytoplankton dynamics within 37 Antarctic coastal polynya systems. *J. Geophys. Res.*, 108, 3271 <https://doi.org/10.1029/2002jc001739>, 2003.

Arthur, J. F., Stokes, C. R., Jamieson, S. S. R., Miles, B. W. J., Carr, J. R., and Leeson, A. A.: The triggers of the disaggregation of Voveykov Ice Shelf (2007), Wilkes Land, East Antarctica, and its subsequent evolution. *J. Glaciol.* <https://doi.org/10.1017/jog.2021.45>, 2021.

Assmann, K. M., Hellmer, H. H., and Jacobs, S. S.: Amundsen Sea ice production and transport. *J. Geophys. Res.*, 110, C12013. <https://doi.org/10.1029/2004JC002797>, 2005.

Banwell, A. F., Willis, I. C., Macdonald, G. J., Goodsell, B., Mayer, D. P., Powell, A., and MacAyeal, D. R.: Calving and rifting on the McMurdo Ice Shelf, Antarctica. *Ann. Glaciol.*, 58, 78–87. <https://doi.org/10.1017/aog.2017.12>, 2017.

Bett, D. T., Holland, P. R., Naveira Garabato, A. C., Jenkins, A., Dutrieux, P., Kimura, S., and Fleming, A.: The impact of the Amundsen Sea freshwater balance on ocean melting of the West Antarctic Ice Sheet. *J. Geophys. Res.: Oceans*, 125, e2020JC016305. <https://doi.org/10.1029/2020JC016305>, 2020.

Bracegirdle, T. J.: Climatology and recent increase of westerly winds over the Amundsen Sea derived from six reanalyses. *Int. J. Climatol.*, 33, 843–851. <https://doi.org/10.1002/joc.3473>, 2013.

Bromwich, D. H. and Kurtz, D. D.: Katabatic wind forcing of the Terra Nova Bay polynya. *J. Geophys. Res.*, 89, 3561. <https://doi.org/10.1029/JC089iC03p03561>, 1984.

1016 Bromwich, D., Liu, Z., Rogers, A. N., and Van Woert, M. L.: Winter atmospheric forcing of the Ross Sea polynya.
1017 Ocean ICE Atmos. Int. Antarct. Cont. Margin, 75, 101-133. <https://doi.org/10.1029/AR075p0101>, 1998.
1018
1019 Bromwich, D. H., Carrasco, J. F., Liu, Z., and Tzeng, R. Y.: Hemispheric atmospheric variations and oceanographic
1020 impacts associated with katabatic surges across the ross ice shelf, Antarctica. J. Geophys. Res.-Atmos, 98, 13045-
1021 13062. <https://doi.org/10.1029/93JD00562>, 1993.
1022
1023 Budge, J. S. and Long, D. G.: A comprehensive database for Antarctic iceberg tracking using scatterometer data.
1024 IEEE JSTARS 11(2), 434-442. <https://10.0.4.85/JSTARS.2017.2784186>, 2018.
1025
1026 Cheng, Z., Pang, X., Zhao, X., and Tan, C.: Spatio-Temporal Variability and Model Parameter Sensitivity Analysis
1027 of Ice Production in Ross Ice Shelf Polynya from 2003 to 2015. Remote Sensing, 9, 934.
1028 <https://doi.org/10.3390/rs9090934>, 2017.
1029
1030 Cheng, Z., Pang, X., Zhao, X., and Stein, A.: Heat Flux Sources Analysis to the Ross Ice Shelf Polynya Ice Production
1031 Time Series and the Impact of Wind Forcing, Remote Sensing, 11, 188. <https://doi.org/10.3390/rs11020188>,
1032 2019.
1033
1034 Dai, L., Xie, H., Ackley, S. F., and Mestas-Nuñez, A. M.: Ice Production in Ross Ice Shelf Polynyas during 2017–
1035 2018 from Sentinel-1 SAR Images. Remote Sensing, 12, 1484. <https://doi.org/10.3390/rs12091484>, 2020.
1036
1037 Doherty, B. T. and Kester, D. R.: Freezing Point of Seawater. J. Mar. Res., 32, 285-300. 1974.
1038
1039 Drucker, R., Martin, S., and Kwok, R.: Sea ice production and export from coastal polynyas in the Weddell and
1040 Ross Seas. Geophys. Res. Lett., 38, L1705. <https://doi.org/10.1029/2011GL048668>, 2011.
1041
1042 [Environment Canada.: Manual of Standard Procedures for Observing and Reporting Ice Conditions \(MANICE\), Me-
1043 teorological Service of Canada, 2005. \[Available at: \[https://publications.gc.ca/collections/collection_2013/ec/En56-
1044 175-2005-eng.pdf\]\(https://publications.gc.ca/collections/collection_2013/ec/En56-175-2005-eng.pdf\)\]](https://publications.gc.ca/collections/collection_2013/ec/En56-175-2005-eng.pdf)
1045
1046 Greene, C. E., Young, D. A., Gwyther, D. E., Galton-Fenzi, B. E., and Blankenship, D. D.: Seasonal dynamics of
1047 Totten Ice Shelf controlled by sea ice buttressing. Cryosphere, 12, 2869-2882. [https://doi.org/10.5194/tc-12-2869-
1048 2018](https://doi.org/10.5194/tc-12-2869-2018), 2018.
1049
1050 Grossmann, S. and Dieckmann, G. S.: Bacterial Standing Stock, Activity, and Carbon Production during Formation
1051 and Growth of Sea–Ice in the Weddell Sea, Antarctica. Appl. Environ. Microb., 60, 2746–2753.
1052 <https://doi.org/10.1128/aem.60.8.2746-2753.1994>, 1994.
1053
1054 Hersbach, H., Bell, B., Berrisford, P., Biavati, G., Horányi, A., Muñoz Sabater, J., Nicolas, J., Peubey, C., Radu, R.,
1055 Rozum, I., Schepers, D., Simmons, A., Soci, C., Dee, D., and Thépaut, J.-N.: ERA5 monthly averaged data on single
1056 levels from 1979 to present. Copernicus Climate Change Service (C3S) Climate Data Store (CDS). (Accessed on <
1057 01-04-2021), <https://doi.org/10.24381/cds.fl7050d7>, 2019.
1058
1059 Hollands, T. and Dierking, W.: Dynamics of the Terra Nova Bay Polynya: The potential of multi-sensor satellite
1060 observations, Remote Sens. Environ., 187, 30–48, <https://doi.org/10.1016/j.rse.2016.10.003>, 2016
1061
1062 IMBIE team: Mass balance of the Antarctic ice sheet from 1992 to 2017. Nature 558, 219-222.
1063 <https://doi.org/10.1038/s41586-018-0179-y>, 2018.
1064
1065 Ito, M., Ohshima, K. I., Fukamachi, Y., Mizuta, G., Kusumoto, Y., and Nishioka, J.: Observations of frazil ice forma-
1066 tion and upward sediment transport in the Sea of Okhotsk: A possible mechanism of iron supply to sea ice. J. Ge-
1067 ophys. Res.–Oceans, 122, 788–802. <https://doi.org/10.1002/2016JC012198>, 2017.
1068
1069 Kim, C.-S., Kim, K.-W., Cho, K.-H., Ha, H. K., Lee, S.H., Kim, H.-C., Lee, J.-H.: Variability of the Antarctic
1070 Coastal Current in the Amundsen Sea. Estuar. Coast. Shelf S., 181, 123–133,
1071 <https://doi.org/10.1016/j.ecss.2016.08.004>, 2016.

Deleted: .

1073
1074 Kimura, N. and Wakatsuchi, M.: Increase and decrease of sea ice area in the Sea of Okhotsk: Ice production in
1075 coastal polynyas and dynamic thickening in convergence zones. *J. Geophys. Res.-Oceans*, 109, C09S03.
1076 <https://doi.org/10.1029/2003JC001901>, 2004.
1077
1078 Koo, Y., Xie, H., Ackley, S. F., Mestas-Nuñez, A. M., Macdonald, G. J., and Hyun, C.-U.: Semi-automated tracking
1079 of iceberg B43 using Sentinel-1 SAR images via Google Earth Engine. *Cryosphere*, 15, 4727–4744,
1080 <https://doi.org/10.5194/tc-15-4727-2021>, 2021.
1081
1082 Lee, S.H., Hwang, J., Ducklow, H. W., Hahm, D., Lee, S. H., Kim, D., Hyun, J.-H., Park, J., Ha, H. K., Kim, T. W.,
1083 Yang, E. J., Shin, H. C.: Evidence of minimal carbon sequestration in the productive Amundsen Sea polynya, *Ge-*
1084 *ophys. Res. Lett.*, 44, 15, 7892-7899. <https://doi.org/10.1002/2017GL074646>, 2017.
1085
1086 Massom, R. A., Hill, K. L., Lytle, V. I., Worby, A.P., Paget, M. J., and Allison, I.: Effects of regional fast-ice and
1087 iceberg distributions on the behaviour of the Mertz Glacier polynya, East Antarctica. *Ann. Glaciol.*, 33, 391-398.
1088 <https://doi.org/10.3189/172756401781818518>, 2001.
1089
1090 Massom, R. A., Scambos, T. A., Bennetts, L. G., Reid, P., Squire, V. A., and Stammerjohn, S. E.: Antarctic ice shelf
1091 disintegration triggered by sea ice loss and ocean swell. *Nature*, 558, 383-389. [https://doi.org/10.1038/s41586-018-](https://doi.org/10.1038/s41586-018-0212-1)
1092 [0212-1](https://doi.org/10.1038/s41586-018-0212-1), 2018.
1093
1094 Matsuoka, K., Skoglund, A., Roth, G., de Pomereu, J., Griffiths, H., Headland, R., Herried, B., Katsumata, K., Le
1095 Brocq, A., Licht, K., Morgan, F., Neff, P. D., Ritz, C., Scheinert, M., Tamura, T., Van de Putte, A., van den Broeke,
1096 M., von Deschanden, A., Deschamps-Berger, C., Van Liefferinge, B., Tronstad, S., and Melvær, Y.: Quantarctica,
1097 an integrated mapping environment for Antarctica, the Southern Ocean, and sub-Antarctic islands. *Environ. Modell.*
1098 *Softw.*, 140, 105015. <https://doi.org/10.1016/j.envsoft.2021.105015>, 2021.
1099
1100 Mazur, A. K., Wählin, A. K., Krężel, A.: An object-based SAR image iceberg detection algorithm applied to the
1101 Amundsen Sea, *Remote Sens. Environ.*, 189, 67–83, <https://doi.org/10.1016/j.rse.2016.11.013>, 2017.
1102
1103 Mazur, A. K., Wählin, A. K., and Kalén, O.: The life cycle of small-to medium-sized icebergs in the Amundsen sea
1104 embayment, *Polar Res.*, 38, 1–17, <https://doi.org/10.33265/polar.v38.3313>, 2019.
1105
1106 [Moore, G. W. K., Howell, S. E. L., and Brady, M.: First observations of a transient polynya in the Last Ice Area](#)
1107 [north of Ellesmere Island. *Geophys. Res. Lett.*, 48, e2021GL095099. <https://doi.org/10.1029/2021GL095099>, 2021.](#)
1108
1109 Morales Maqueda, M. A., Willmott, A. J., and Biggs, N. R. T.: Polynya dynamics: a review of observations and
1110 modeling, *Rev. Geophys.*, 42, RG1004. <https://doi.org/10.1029/2002RG000116>, 2004.
1111
1112 Morelli, S. and Parmiggiani, F.: Wind over Terra Nova Bay (Antarctica) during a polynya event: Eta model simula-
1113 tions and satellite microwave observations. *Eur. Phys. J. Plus* 128, 135 (2013). [https://doi.org/10.1140/epjp/i2013-](https://doi.org/10.1140/epjp/i2013-13135-8)
1114 [13135-8](https://doi.org/10.1140/epjp/i2013-13135-8), 2013.
1115
1116 Morlighem, M.: MEaSUREs BedMachine Antarctica, Version 2. Boulder, Colorado USA. NASA National Snow
1117 and Ice Data Center Distributed Active Archive Center. <https://doi.org/10.5067/C2GFER6PTOS4>, 2019. [Date Ac-
1118 cessed: 01-04-2021].
1119
1120 [Nakata, K., Ohshima, K. I., and Nihashi, S.: Estimation of thin ice thickness and discrimination of ice type from](#)
1121 [AMSR-E passive microwave data. *IEEE TGRS*, 57\(1\), 263–276. <https://doi.org/10.1109/TGRS.2018.2853590>,](#)
1122 [2019.](#)
1123
1124 [Nakata, K., Ohshima, K. I., and Nihashi, S.: Mapping of active frazil for Antarctic coastal polynyas, with an estima-](#)
1125 [tion of sea-ice production. *Geophys. Res. Lett.*, 48, e2020GL091353. <https://doi.org/10.1029/2020GL091353>, 2021.](#)
1126

Deleted: ¶

Field Code Changed

Deleted: iew

Deleted: of

Deleted: ics

Deleted: ¶

Deleted: ¶

1133 Nihashi, S., and Ohshima, K. I.: Circumpolar Mapping of Antarctic Coastal Polynyas and Landfast Sea Ice: Relationship and Variability, *J. Climate*, 28, 3650-3670. <https://doi.org/10.1175/JCLI-D-14-00369.1>, 2015.

1134

1135

1136 Nihashi, S., Ohshima, K. I., and Tamura, T.: Sea-Ice Production in Antarctic Coastal Polynyas Estimated From

1137 AMSR2 Data and Its Validation Using AMSR-E and SSM/I-SSMIS Data. *IEEE JSTARS*, 10, 3912-3922.

1138 <https://doi.org/10.1109/JSTARS.2017.2731995>, 2017.

1139

1140 Ohshima, K. I., Fukamachi, Y., Williams, G. D., Nihashi, S., Roquet, F., Kitade, Y., Tamura, T., Hirano, D., Her-

1141 raiz-Borreguero, L., Field, I., Hindell, M., Aoki, S. and Wakatsuchi, M. L.: Antarctic Bottom Water production by

1142 intense sea-ice formation in the Cape Damley polynya. *Nat. Geosci.*, 6, 235-240. <https://doi.org/10.1038/ngeo1738>,

1143 2013.

1144

1145 Park, J., Kim, H.-C., Jo, Y.-H., Kidwell, A., and Hwang, J.: Multi-temporal variation of the ross sea polynya in re-

1146 sponse to climate forcings. *Polar Res.*, 37, 1444891. <https://doi.org/10.1080/17518369.2018.1444891>, 2018.

1147

1148 Parkinson, C. L.: A 40-y record reveals gradual Antarctic sea ice increases followed by decreases at rates far exceed-

1149 ing the rates seen in the Arctic. *P. Natl. Acad. Sci. U.S.A.*, 116, 14414-14423.

1150 <https://doi.org/10.1073/pnas.1906556116>, 2019.

1151

1152 Parmiggiani, F.: Fluctuations of Terra Nova Bay polynya as observed by active (ASAR) and passive (AMSR-E) mi-

1153 crowave radiometers, *Int. J. Remote. Sens.*, 27:12, 2459-2467. <https://doi.org/10.1080/01431160600554355>, 2007.

1154

1155 Preußner, A., Heinemann, G., Willmes, S., and Paul, S.: Multi-Decadal Variability of Polynya Characteristics and Ice

1156 Production in the North Water Polynya by Means of Passive Microwave and Thermal Infrared Satellite Imagery.

1157 *Remote Sensing*, 7, 15844-15867. <https://doi.org/10.3390/rs71215807>, 2015.

1158

1159 [QGIS.org](http://www.qgis.org): QGIS Geographic Information System. QGIS Association. <http://www.qgis.org>. 2021.

1160

1161 Rack, W., Price, D., Haas, C., Langhorne, P. J., and Leonard, G. H.: Sea Ice Thickness in the Western Ross Sea. *Ge-*

1162 *ophys. Res. Lett.*, 48, e2020GL090866. <https://doi.org/10.1029/2020GL090866>, 2020.

1163

1164 Rignot, E., Mouginot, J., Scheuchl, B., van den Broeke, M., van Wessem, M. J., and Morlighem, M.: Four decades

1165 of Antarctic ice sheet mass balance from 1979–2017. *P. Natl. Acad. Sci. U.S.A.* 116, 1095-1103.

1166 <https://doi.org/10.1073/pnas.1812883116>, 2019.

1167

1168 Sansiviero, M., Morales Maqueda, M. Á., Fusco, G., Aulicino, G., Flocco, D., and Budillon, G.: Modelling sea ice

1169 formation in the Terra Nova Bay polynya. *J. Marine Syst.*, 166, 4-25. <https://doi.org/10.1016/j.jmarsys.2016.06.013>,

1170 2017.

1171

1172 Spreen, G., Kaleschke, G. L., and Heygster, G.: Sea ice remote sensing using AMSR-E 89 GHz channels. *J. Geophys.*

1173 *Res.*, 113, C02S03. <https://doi.org/10.1029/2005JC003384>, 2008.

1174

1175 Stammerjohn, S. E., Maksym, T., Massom, R. A., Lowry, K. E., Arrigo, K. R., Yuan, X., Raphael, M., Randall-

1176 Goodwin, E. R., Sherrell, R. M., and Yager, P. L.: Seasonal sea ice changes in the Amundsen Sea, Antarctica, over

1177 the period of 1979–2014. *Elementa: Science of the Anthropocene*, 3, 000055. <https://doi.org/10.12952/journal.elementa.000055>, 2015.

1178

1179

1180 St-Laurent, P., Yager, P. L., Sherrell, R. M., Stammerjohn, S. E., and Dinniman, M. S.: Pathways and supply of dis-

1181 solved iron in the Amundsen Sea (Antarctica), *J. Geophys. Res.-Oceans*, 122, 7135–7162, <https://doi.org/10.1002/2017JC013162>, 2017.

1182

1183

1184 St-Laurent, P., Yager, P. L., Sherrell, R. M., Oliver, H., Dinniman, M. S., and Stammerjohn, S. E.: Modeling the

1185 seasonal cycle of iron and carbon fluxes in the Amundsen Sea Polynya, Antarctica. *J. Geophys. Res.: Oceans*, 124,

1186 1544–1565. <https://doi.org/10.1029/2018JC014773>, 2019.

1187

1188 Sweeney, C.: The annual cycle of surface water CO₂ and O₂ in the Ross Sea: A model for gas exchange on the con-
1189 tinental shelves of Antarctica, in Biogeochemistry of the Ross Sea. Antarctica Research Series, 78, edited by Dun-
1190 bar, R. B., and DiTullio, G. R., pp. 295-312, AGU, Washington, D. C., 2003.
1191
1192 Tamura, T., Ohshima, K. I., and Nihashi, S.: Mapping of sea ice production for Antarctic coastal polynyas, Ge-
1193 ophys. Res. Lett., 35, L07606. <https://doi.org/10.1029/2007GL03290>, 2008.
1194
1195 Tamura, T., Williams, G. D., Fraser, A. D., and Ohshima, K. I.: Potential regime shift in decreased sea ice produc-
1196 tion after the Mertz Glacier calving. Nat. Commun., 3, 826. <https://doi.org/10.1038/ncomms1820>, 2012.
1197
1198 Tian, L., Xie, H., Ackley, S. F., Tang, J., Mestas-Nuñez, A. M., and Wang, X.: Sea-ice freeboard and thickness in
1199 the Ross Sea from airborne (IceBridge 2013) and satellite (ICESat 2003-2008) observations. Ann. Glaciol., 61(82),
1200 24-39. <https://doi.org/10.1017/aog.2019.49>, 2020.
1201
1202 Webber, B. G. M., Heywood, K. J., Stevens, D. P., Dutrieux, P., Povl Abrahamsen, E., Jenkins, A., Jacobs, S. S.,
1203 Ha, H. K., Lee, S. H., and Kim, T. W.: Mechanisms driving variability in the ocean forcing of Pine Island Glacier,
1204 Nat. Commun., 8, 14507. <https://doi.org/10.1038/ncomms14507>, 2017.